Available online at www.sciencedirect.com

ScienceDirect

Advances in Space Research 76 (2025) 1832–1853

ADVANCES IN SPACE RESEARCH (a COSPAR publication)

www.elsevier.com/locate/asr

# Temporal variability in low-frequency radio interference: Insight from high-cadence monitoring at a candidate radio notification zone in Malaysia

Affan Adly Nazri [a], Zamri Zainal Abidin [a,*], Mohamad Ridhauddin Mat Sabri [a], Zulfazli Rosli [a,b], Mohd Shaiful Rizal Hassan [a], Mohd Shazwan Mohd Radzi [a], Ahmad Najwan Zulkiplee [a], Dalilah Nur Fathiah Hanim Razak [a], Norsyazwani Asmi [a], Jinsong Ping [c], Mingyuan Wang [c], Liang Dong [d,e]

[a] *Radio Cosmology Research Lab, Centre for Astronomy and Astrophysics Research, Department of Physics, Faculty of Science, Universiti Malaya, Kuala Lumpur 50603 Kuala Lumpur, Malaysia*

[b] *Centre of Foundation, Language and Malaysian Studies, Universiti Malaya-Wales, Kuala Lumpur 50480, Malaysia*

[c] *National Astronomical Observatories, Chinese Academy of Sciences, Beijing 100012, China*

[d] *Yunnan Astronomical Observatory, Chinese Academy of Sciences, Kunming650216, China*

[e] *Yunnan Sino-Malaysian International Joint Laboratory of HF-VHF Advanced Radio Astronomy Technology, Kunming 650216, China*

Received 16 January 2025; received in revised form 1 May 2025; accepted 11 May 2025
Available online 14 May 2025

**Abstract**

Extensive radio frequency interference (RFI) monitoring is essential in the site selection process before constructing radio astronomy observatories, followed by mitigation strategies to minimize its adverse effects. Malaysia has an enormous prospect for radio astronomy due to its prominent location in the centre of Southeast Asia, but is challenged by its relatively high population density. In this research article, we perform high-cadence, low-frequency RFI monitoring at two sites, each representing an urban and a rural environment. Using modified generalized spectral kurtosis (GSK) as an RFI detection method, we ascertain the suitability of Glami Lemi, a rural area in the centre of Peninsular Malaysia previously assigned as a candidate radio notification zone (RNZ), as a potential site for radio astronomy observations due to its lower RFI contamination in our high-cadence monitoring, especially when compared with urban areas. We identified a number of persistent and transient RFI in our dataset, associate each of them with their potential origins and, if present, characterize their temporal evolution. A few types of RFI mitigation strategies were also tested and discussed. This study lays the groundwork for Malaysia's endeavours in establishing its first research-grade radio telescope, emphasizing the importance of robust RFI detection and mitigation strategies in optimizing observational outcomes.


*Keywords:* Radio astronomy; Radio frequency interference; Higher-order statistics

## 1. Introduction

In modern astrophysics, observations across the entire electromagnetic spectrum ranging from radio and microwave to infrared, optical, ultraviolet, X-rays, and

* Corresponding author.
*E-mail addresses:* affanadly.astro@gmail.com (A.A. Nazri), zzaa@um.edu.my (Z.Z. Abidin).

https://doi.org/10.1016/j.asr.2025.05.035

gamma-rays play crucial roles in building a comprehensive understanding of the Universe. Each regime probes distinct physical regimes, offering complementary perspective on astrophysical objects. While historically associated with cold, low-energy processes, radio observations now play a central role in exploring some of the Universe's most extreme and energetic phenomena – including pulsars, supernova remnants, and fast radio bursts. The development of radio interferometry, especially Very Long Baseline Interferometry (VLBI), further enables extremely high-resolution and sensitive observations by combining signals from radio telescopes separated by large distances. VLBI has since been able to confirm various astrophysical phenomena that were once only predicted by theories e.g. event horizon of supermassive black holes (Akiyama et al., 2019), and spiral arms in accretion disk of massive protostars (Burns et al., 2023).

Radio frequencies are divided into multiple frequency bands (See Section 5.3.1; International Telecommunication Union, 2015), and a portion of the bands, namely the low frequency (LF), medium frequency (MF), high frequency (HF), and very high frequency (VHF), span over 30 kHz – 300 MHz, are crucial for various sciences in radio astronomy, including solar activity monitoring (solar burst and solar flares) and space weather observations, deep extragalactic observations of active galactic nuclei (AGNs), galaxies, and galaxy clusters, high-redshift observations, cosmic ray observations, and pulsar monitoring. Many instruments have been deployed to harness these frequencies[1], mainly interferometers such as the Very Large Array (VLA; 300–350 MHz and 74 MHz; Thompson et al., 1980; Kassim et al., 1993), the Low-Frequency Array (LOFAR; 10 –240 MHz; van Haarlem et al., 2013), the 21 CentiMeter Array (21CMA; 50 – 200 MHz; Zhao et al., 2022), the Murchison Widefield Array (MWA; 70 – 300 MHz; Lonsdale et al., 2009), the Giant Metrewave Radio Telescope (GMRT; 150 – 1450 MHz; Gupta et al., 2017), and the upcoming Square Kilometre Array Low Frequency Telescope (SKA-low; 50 – 350 MHz; Labate et al., 2022).

However, astrophysical sources are usually masked over by terrestrial radio signals (e.g. telecommunications) due to their significantly lower power. These terrestrial signals are referred to as radio frequency interference (RFI) and pose a danger to radio astronomical observations. Although RFI can occur across the entire radio spectrum, it is particularly prevalent and problematic at lower frequencies (Bentum and Boonstra, 2011). One solution is to build radio telescopes in radio quiet zones (RQZ) and radio notification zones (RNZ), but in countries with a majority of high and medium population density such as Malaysia, RFI evaluation becomes an extremely crucial procedure (Abidin et al., 2012; Abidin et al., 2021). In addition to terrestrial sources, another emerging concern is the unintended interference from satellite constellations in low Earth orbit (LEO) e.g. Starlink. These satellites have been seen to affect frequencies used for radio astronomy, and its absence in RQZ regulations means that coexistence strategies are required even in remote or protected regions (Di Vruno et al., 2023).

This paper aims to investigate low frequency RFI in two locations within Malaysia; each representing an urban and rural environments. Malaysia's location close to the equator would allow for a wide sky coverage in both celestial hemispheres, which is currently covered by few, if not any radio telescope(s). Its central location in Southeast Asia would also significantly benefit VLBI experiments by serving as a vital link between the East Asian VLBI Network (EAVN; comprising of China, Korea, and Japan) and the Long Baseline Array (LBA; i.e. Australian telescopes/arrays), and even the European VLBI Network (EVN). This connection would enhance the overall network's performance, particularly by improving short baselines and increasing overall sensitivity. Ultimately, alongside Thailand, Indonesia and Vietnam, involvement of Malaysia would further develop the goal of the regional South East Asian VLBI Network (SEAVN; Sugiyama et al., 2022).

We organise this paper as follows: Section 2 serves as a mini review of previous RFI monitoring that have been performed in Malaysia. Section 3 summarizes the Generalized Spectral Kurtosis method which is used here for RFI detection. Section 4 describes the instrumentation, observational parameters, and data analysis procedures. The results of the RFI monitoring are then presented in Section 5, along with associations of the RFI detected with spectrum allocations, potential origins, and presence of physical phenomena. Finally, we present and test a few potential RFI mitigation techniques in Section 6.

## 2. Previous RFI monitoring works in Malaysia

RFI monitoring in Malaysia began as a pilot project for the establishment of radio astronomy research in the country. Naturally, these projects were performed in/near research institutes which are mainly located in dense populations such as in Universiti Malaya, Universiti Sultan Zainal Abidin, Universiti Teknologi MARA, Universiti Pendidikan Sultan Idris, and Universiti Kebangsaan Malaysia (Abidin et al., 2009; Hamidi et al., 2011; Hamidi et al., 2012a; Umar et al., 2015; Zavvari et al., 2015). As expected, most of these locations suffer from very high RFI, mainly due to mobile telecommunication, broadcasting (radio and television) and satellite communications (Abidin et al., 2009; Abidin et al., 2010; Hamidi et al., 2011). These RFI measurements targeted wide bands of up to 2.8 GHz, covering a number of important radio astronomy bands as shown in Table 1.

[1] Although the International Telecommunication Union (ITU) defines this frequency range as low- to very-high frequencies, they are commonly referred to as *low frequencies* in astronomy and astrophysics. Therefore, throughout the paper, we adopt the latter definition unless explicitly mentioned.

Table 1
Important frequency bands used in radio astronomy below 2.8 GHz (Sources: Abidin et al., 2009; International Telecommunication Union, 2013).

| Frequency range (MHz) | Radio astronomy usage |
|---|---|
| 13.36–13.41 | Solar observation |
| 25.55–25.67 | Jupiter observation |
| 37.50–38.25 | Continuum observation |
| 73.00–74.60 | Solar wind measurement |
| 150.05–153.00 | Pulsar monitoring |
| 322.00–328.85 | Deuterium observation |
| 406.00–410.00 | Pulsar monitoring |
| 608.00–614.00 | Continuum and interferometry |
| 1400.00–1427.00 | 21-cm hydrogen observation |
| 1610.60–1613.80 | Hydroxyl observation |
| 1660.00–1670.00 | Hydroxyl observation |
| 1718.80–1722.20 | Hydroxyl observation |
| 2655.00–2700.00 | Pulsar monitoring and interferometry |

Further research by Abidin et al. (2013) and Umar et al. (2014) documented the influence of population density on RFI levels. Correlation between the noise levels and population density was seen, largely due to the heavy contamination from telecommunication services in urban areas. Emissions of these sources typically appear between 900–1200 MHz and 1600–2000 MHz (Abidin et al., 2009; Hamidi et al., 2011; Hamidi et al., 2012a; Hamidi et al., 2012b). This suggests that radio telescopes should ideally be built in sparsely populated regions, with a suggested population density threshold of 150 people per square kilometre[2] (Umar et al., 2014).

Following that, various rural areas in Malaysia (e.g. Jelebu, Sekayu, Langkawi, Behrang, Merang; Abidin et al., 2010; Abidin et al., 2011; Umar et al., 2012; Noorazlan et al., 2013; Zafar et al., 2017; Shafie et al., 2017; Zafar et al., 2018; Shafie et al., 2021) were explored and notably lower RFI levels were detected, with exceptions in satellite and broadcasting frequency bands. Observations in narrow spectral windows (e.g. deuterium, 21-cm hydrogen, hydroxyl) reveal mixed results – few locations show absence of RFI in certain bands (e.g. deuterium; Zavvari et al., 2015), while others display RFI spilling into the vicinity of important bands (e.g. hydroxyl; Zavvari et al., 2015) or even contaminating the band itself (e.g. deuterium; Abidin et al. (2012), and L-band; Abidin et al. (2013); Zafar et al. (2017)).

The current most comprehensive RFI study conducted in Peninsular Malaysia aimed to investigate radio quiet zones (RQZ) and radio notification zones (RNZ). Abidin et al. (2021) stated that although RQZs are ideal locations for radio astronomy, they are both logistically impractical and almost impossible to realize in a dense population like Malaysia. RNZs become the next best option where there are no authoritative restrictions, but shared frequencies are *notified* to the corresponding parties. They listed five RQZ and two RNZ candidates (with Universiti Malaya as a reference) based on average monthly humidity/rainfall, population density, and distance from mobile and broadcasting stations using the minimum weightage method. Shown in Fig. 1 is a map of the candidate RNZs and RQZs with the minimum weightage boundaries. When RFI monitoring was performed up to 4 GHz, they found that the average noise in all the sites are below the International Telecommunication Union (ITU) recommendation for continuum and spectral line astronomy observations[3], with Kuala Tembeling and Jelebu regarded as the best RQZ and RNZ sites respectively.

However, most of these measurements were performed with various limitations. Firstly, most observations cover very wide frequency ranges of up to 9 GHz, resulting in a large band separations which may not capture narrow band RFI (e.g. Abidin et al., 2012). Narrow band RFI measurements in contrast target frequencies above VHF VLBI windows or specific spectral lines. Basic and small antennas (9" omnidirectional, 5.2 cm discones, and 50 cm Yagi antennas) which were used may also miss weaker RFI signals that would otherwise be captured by sensitive radio telescopes (e.g. Noorazlan et al., 2013). In addition, the RFI data were taken over large cadences and averaged, meaning that transient RFI emissions cannot be studied (except in Abidin et al. (2011), but no detailed results were discussed). Finally, majority of the studies perform little to no statistical evaluations (e.g. only using noise average and standard deviations) which may not manifest the true nature of the RFI. Only in a few cases (e.g. Abidin et al., 2011; Noorazlan et al., 2013; Zafar et al., 2017), higher order Kurtosis statistics were utilized, but exclusively in the temporal domain and were not discussed in detail.

## 3. Generalized Spectral Kurtosis (GSK)

Nita et al. (2007) proposed the spectral kurtosis (SK) estimator method to detect (and mitigate) RFI in real time. The generalized spectral kurtosis (GSK) was then introduced by Nita and Gary (2010a), a method that interposes the time-averaging factor to address hardware limitations of standard correlators. Generalizing the shape factor in the gamma distribution obeyed by the power spectrum allows it to be applied to instruments which can only output already averaged data. These methods have been applied to various instruments with noteworthy performance e.g. the Korean Solar Radio Burst Locator (KBRSL; Dou et al., 2009), the Expanded Owens Valley Solar Array (EOVSA; Nita et al., 2016b), the Canadian Hydrogen Intensity Mapping Experiment instrument (CHIME; Taylor et al., 2019), and the Parkes Telescope

[2] Depending on the advancement of technology and its prevalence in the common household, the population density threshold will vary across time.

[3] ITU-R RA.769–2: Protection criteria used for radio astronomical measurements.

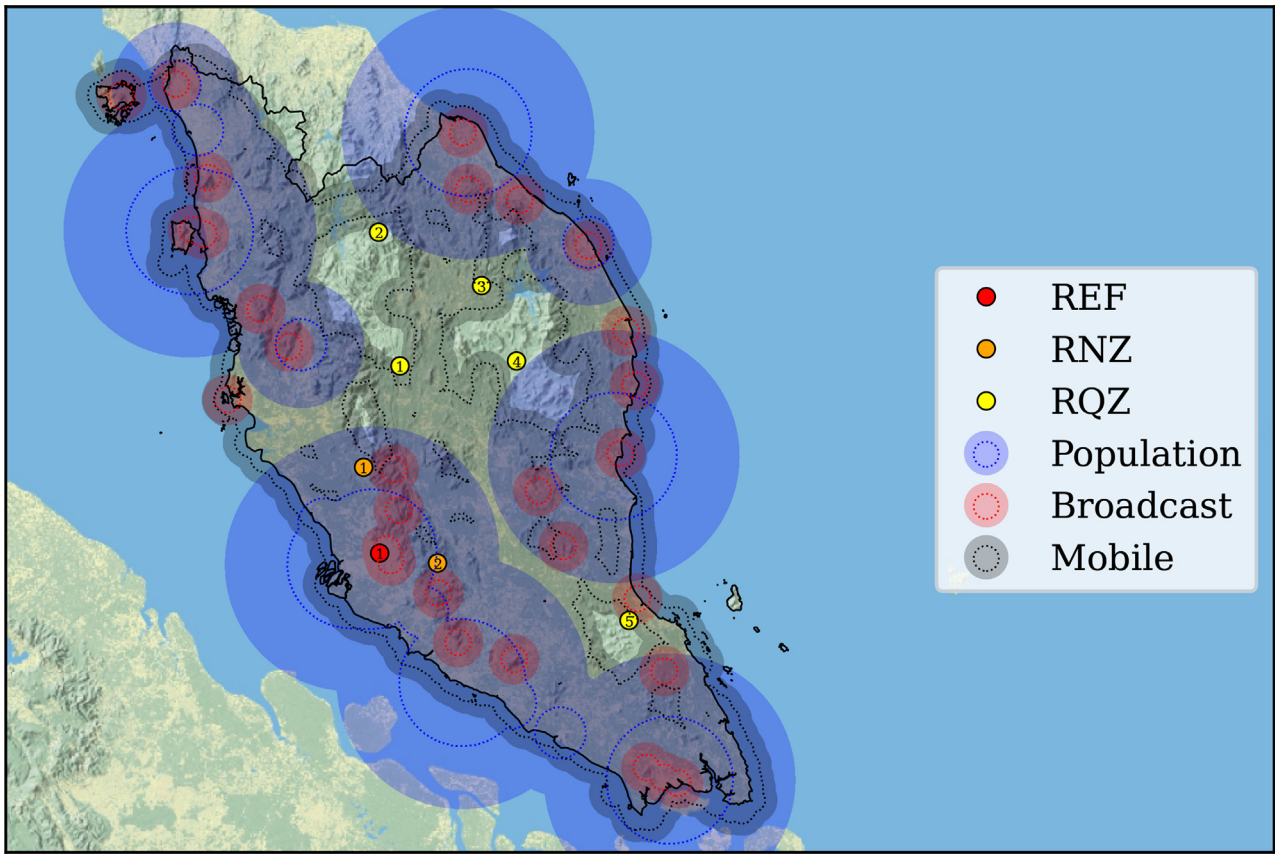


Fig. 1. Identification of possible RNZs and RQZs in Peninsular Malaysia based on the minimum weightage method as described in Abidin et al. (2021). The coloured semi-transparent areas denote the RQZ-defined contamination range, while the dotted lines within them denote the RNZ-defined contamination range, each for population densities displayed in blue, or for each type of RFI source i.e. broadcasting stations (TV, AM, and FM) in red, and mobile telecommunication (2G, 3G, and 4G) in grey. The red, orange, and yellow points indicate the locations of reference (1: Universiti Malaya), candidate RNZ (1: Universiti Pendidikan Sultan Idris, 2: Jelebu), and candidate RQZ (1: Kuala Medang, 2: Grik, 3: Gua Musang, 4: Kuala Tembeling, 5: Selendang) sites respectively i.e. where the RFI monitorings were performed in Abidin et al. (2021). Note that the population data, and mobile and broadcast station locations have been updated to the latest available data, and this may have redacted the RNZ and RQZ status of a few sites (namely Universiti Pendidikan Sultan Idris, Gua Musang,. and Selendang).

(Wongphechauxsorn et al., 2023). This method has also been evaluated to be effective for cross-correlation application, potentially applicable in VLBI (Nita and Hellbourg, 2020). SK's simplicity further allows for real-time calculations and application on radio receivers using low-cost FPGAs (Quirós-Olozábal et al., 2016; Taylor et al., 2019).

As described by Nita and Gary (2010a), the GSK estimator is defined by

$$\widehat{SK} = \frac{MNd+1}{M-1}\left(\frac{MS_2}{S_1}-1\right) \tag{1}$$

where $S_1 = \sum_{i=1}^{M}\left(\sum_{j=1}^{N} x_j\right)_i, S_2 = \sum_{i=1}^{M}\left(\sum_{j=1}^{N} x_j\right)_i^2$, and $M, N$, and $d$ are the accumulation length of power spectral density $x_i$, number of averaged spectra prior to recording, and shape factor (explained later in Section 4.3) respectively. The mean and first central moments of the pdf of $\widehat{SK}$ can then be analytically defined based on Eq. 1 (refer Nita and Gary, 2010b) as

$$\mu_1 = E\left(\widehat{SK}\right) \equiv 1$$

$$\mu_2 = \frac{2Nd(Nd+1)M^2\Gamma(MNd+2)}{(M-1)\Gamma(MNd+4)}$$

$$\mu_3 = \frac{8Nd(Nd+1)M^3\Gamma(MNd+2)}{(M-1)^2\Gamma(MNd+6)} \times\left[(Nd+4)MNd-5Nd-2\right]$$

$$\mu_4 = \frac{12Nd(Nd+1)M^4\Gamma(MNd+2)}{(M-1)^3\Gamma(MNd+8)} \times\left(M^3N^4d^4+3M^2N^4d^4+M^3N^3d^3 +68M^2N^3d^3 -93MN^3d^3+125M^2N^2d^2-245MN^2d^2 +84N^2d^2-32MNd+48Nd+24\right).$$

where $\Gamma$ is the gamma function. Notice that the GSK estimator has a mean of 1, and this eliminates the need for the evaluation of the mean background level which can be skewed in the presence of strong RFI.

To approximate the SK distribution, we utilize the Pearson Type III probability distribution function (pdf), which follows the generally asymmetrical frequency curve of background radio emissions in nature (Pearson and Henrici, 1895). The Type III cumulative function (CF) is consequently defined as

$$CF(\xi,\alpha,\beta,\delta)=\Gamma_x\left(\beta,\frac{\xi-\delta}{\alpha}\right)/\Gamma(\beta) \tag{2}$$

where $\alpha=\mu_3/2\mu_2, \beta=4\mu_2^3/\mu_3^2, \delta=1-2\mu_2^2,$ and $\Gamma_x(\beta,x)=\int_0^x t^{\beta-1}e^{-t}\,dt$ is the incomplete gamma function. This approximation is accurate up to the third order, especially for large accumulation lengths $M>1000$ (Nita and Gary, 2010a). By setting a predefined false alarm probability $P_{\rm FA}$ (usually 0.13499% which is equivalent to the $P_{\rm FA}$ of a $3\sigma$ threshold applied to a Gaussian distribution), one can ultimately obtain the bounds of good $\widehat{SK}$ (denoted as $\delta_{\rm lower}$ and $\delta_{\rm upper}$) by optimizing the $P_{\rm FA}$ with the Type III CF and complementary CF, and then flag the respective channels in the data accordingly.

## 4. Methodology

### 4.1. Instruments

Our observational setup consists of two main instruments – A dual-polarization logarithmic periodic antenna and a Liquid Instruments Moku:Lab.

The dual-polarization logarithmic periodic antenna consists of two log-periodic antennas arranged perpendicularly along their principle axis, allowing it to measure two linear polarizations at once (horizontal and vertical). The antenna has a total length of 180 cm and a width of 202 cm, equipped with a total of 17 dipoles with a standing wave ratio of 2.5. The antenna operates optimally up to 1000 MHz, with a typical gain of 6.5 dBi and input impedance of 50Ω. At 100 MHz, the antenna has a beamwidth of 118.6° and 60.4° in the H- and E-planes respectively.

The Liquid Instruments Moku:Lab is a reconfigurable hardware platform mainly controlled by Field Programmable Gate Arrays (FPGA), and equipped with multiple low-noise analogue inputs and outputs (Liquid Instuments, 2023). In our case, the spectrum analyser mode was used to measure the radio signals from the antenna. Table 2 shows the specifications of the Moku:Lab in the spectrum analyser mode. The instrument's input noise follows the following profile (for $f$ in kHz):

$$S_\eta(f)\approx 13.9\ \text{nV}\times\sqrt{1+\frac{220\ \text{kHz}}{f}} \tag{3}$$

For our observations between $0-250$MHz, the average input noise is approximately 13.6nV, with a noise factor of 2 dB (equivalent to a noise temperature of $\sim$ 170K).

Table 2
Specifications of Moku:Lab in spectrum analyser mode.

| Parameter | Value |
|---|---|
| Frequency range | DC to 250MHz |
| Frequency channels | 1023 |
| Channel spacing | 244140.62Hz |
| Impedance (AC) | 50Ω |
| Attenuation (AC) | 0dB |
| Voltage range | ±0.5V |
| Voltage sensitivity | −130dBm |

### 4.2. Observations

The radio observations were done in two locations. The first location is the Physics Department, Universiti Malaya (UM), located in Malaysia's capital Kuala Lumpur, Malaysia (3°7′23.754″N, 101°39′10.6812″E, 78 m altitude). UM represents a highly populated urban area (Population density: 8235km$^{-2}$), prone to be contaminated by large amounts of RFI. The second location is the Glami Lemi Biotechnology Research Centre (GL), located in Jelebu, Negeri Sembilan, Malaysia (3°3′12.6216″N, 102°3′51.7032″E, 144 m altitude). GL has been suggested as a RNZ due to its low population density (Population density: 35.11km$^{-2}$) and shielding from surrounding hills, and combined with the location's low average humidity and precipitation makes it a prominent location for radio astronomy observations (Abidin et al., 2021). The two locations are marked in the map shown in Fig. 2. The antenna was azimuthally oriented to point away from the largest nearby structure(s) (e.g. buildings, hills/mountains, etc.) to maximize the capture of RFI present in the environment. The observation schedule for both locations are shown in Table 3, and the radio spectrum was obtained approximately every 0.3 s. Fig. 3 shows a side-view of the antenna deployed in one of the observation locations.

### 4.3. Modified GSK estimator

To detect frequency channels contaminated by RFI, we adopt the generalized spectral kurtosis (GSK) method as explained in Section 3. In this work, since the value of $N$ for our instrument is not precisely known, we assume $N$ to have a value of unity, representing unaveraged power spectral density (Smith et al., 2022).

Eq. 1 indicates that the $\widehat{SK}$ spectra will typically appear flat, with the exception of RFI-contaminated frequencies. However, due to variations in instrument characteristics (e.g. digitizer quantization; Nita and Hellbourg, 2020), the $\widehat{SK}$ spectra will not be normalized to unity. To address this, we could normalize the $\widehat{SK}$ spectra by calculating its mean. To be exact, the spectra is normalized using the shape factor (Nita and Hellbourg, 2020) which is defined based on the ideal case of Eq. 1 as

$$d=\frac{M-\mu+1}{M\mu} \tag{4}$$

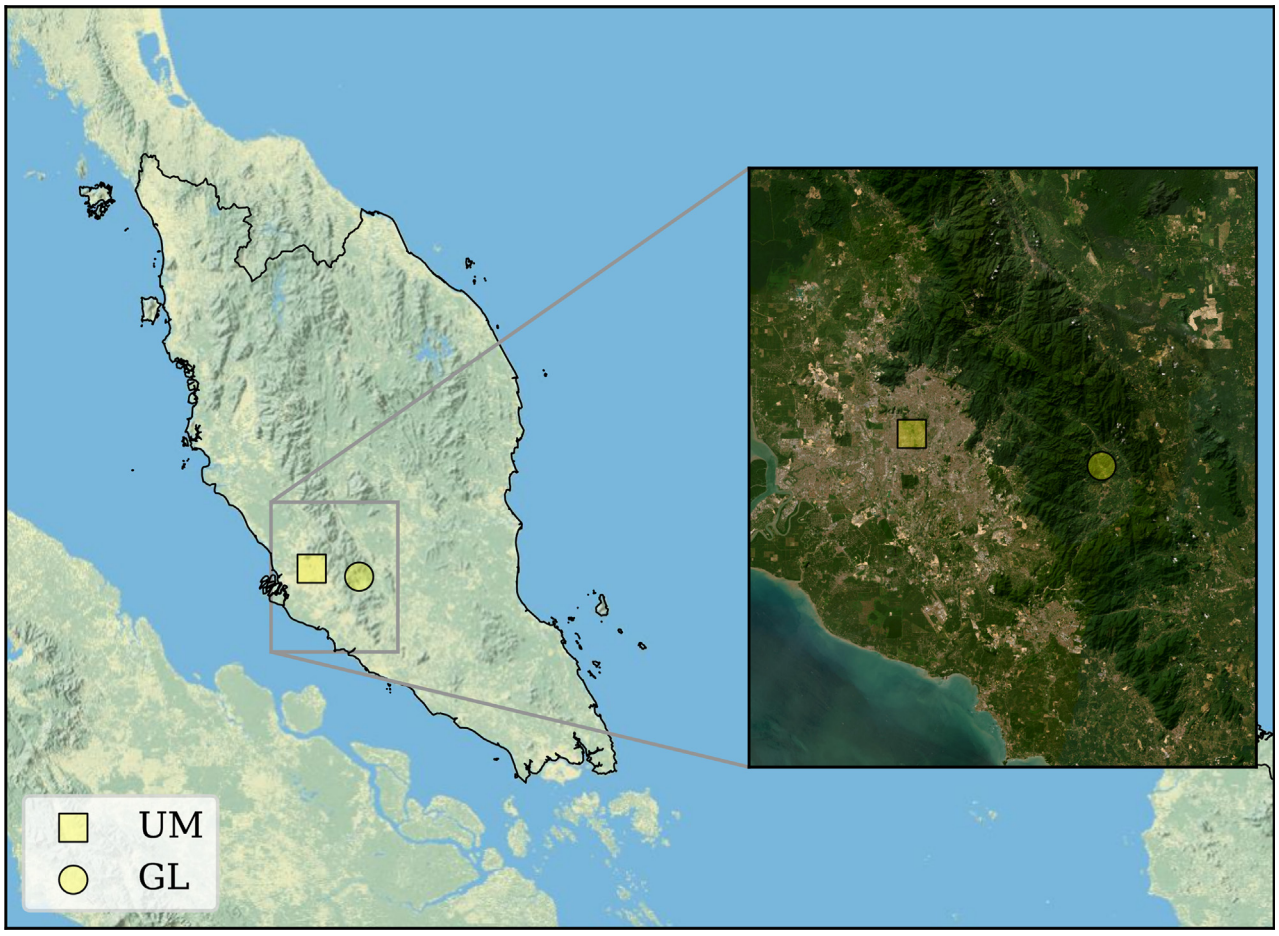


Fig. 2. A map of Peninsular Malaysia with the two radio observation stations. The main map represents the Natural Earth physical map, while the inset shows a zoomed-in satellite image around the two stations, depicting their respective urban and rural environments. The GL station can also be seen to be surrounded by the Titiwangsa Mountains which provides shielding from urban radio signals.

Table 3
Observation schedule. Start and end times are written in GMT + 8 (Malaysian Time).

| Location | Start Date | End Date | Start Time | End Time |
|---|---|---|---|---|
| UM | 2 Nov 2023 | 3 Nov 2023 | 06:08:06 | 06:05:11 |
| GL | 24 Oct 2023 | 25 Oct 2023 | 16:01:05 | 17:00:58 |

where $\mu = \left\langle \widehat{SK}(d \equiv 1) \right\rangle$ i.e. the mean of $\widehat{SK}$. This empirical approach means that the true value of $N$ isn't required as its value will be influenced by the $d$ estimates.

We then propose the usage of the median, $\hat{\mu}$ instead of the mean to calculate the shape factor, modifying Eq. 4 into

$$d = \frac{M - \hat{\mu} + 1}{M\hat{\mu}} \tag{5}$$

This helps to safeguard the integrity of $\widehat{SK}$ from the influence of significantly RFI-contaminated frequencies, assuming that there are more uncontaminated frequencies than contaminated ones.

Similar to the EOVSA (Nita et al., 2016b), the dual-polarization data are flagged separately and then combined using an OR operator. This is done to capture RFIs in each channel and flag them in both linear polarizations without any bias, though this does increase the expected $P_{\mathrm{FA}}$ by a factor of $(2 - P_{\mathrm{FA}})$, for which in the case of the Gaussian $3\sigma$ threshold, to 0.270% (Nita and Hellbourg, 2020).

## 5. Results and discussion

### 5.1. Urban vs rural RFI

Figs. 4 and 5 show the overall result plots for UM and GL data respectively, with the middle panel showing the

Fig. 3. Side-view of the dual-polarization logarithmic periodic antenna set up in GL for radio observation. The two coaxial cables connected to the base of the antenna are connected to the spectrum analyser.

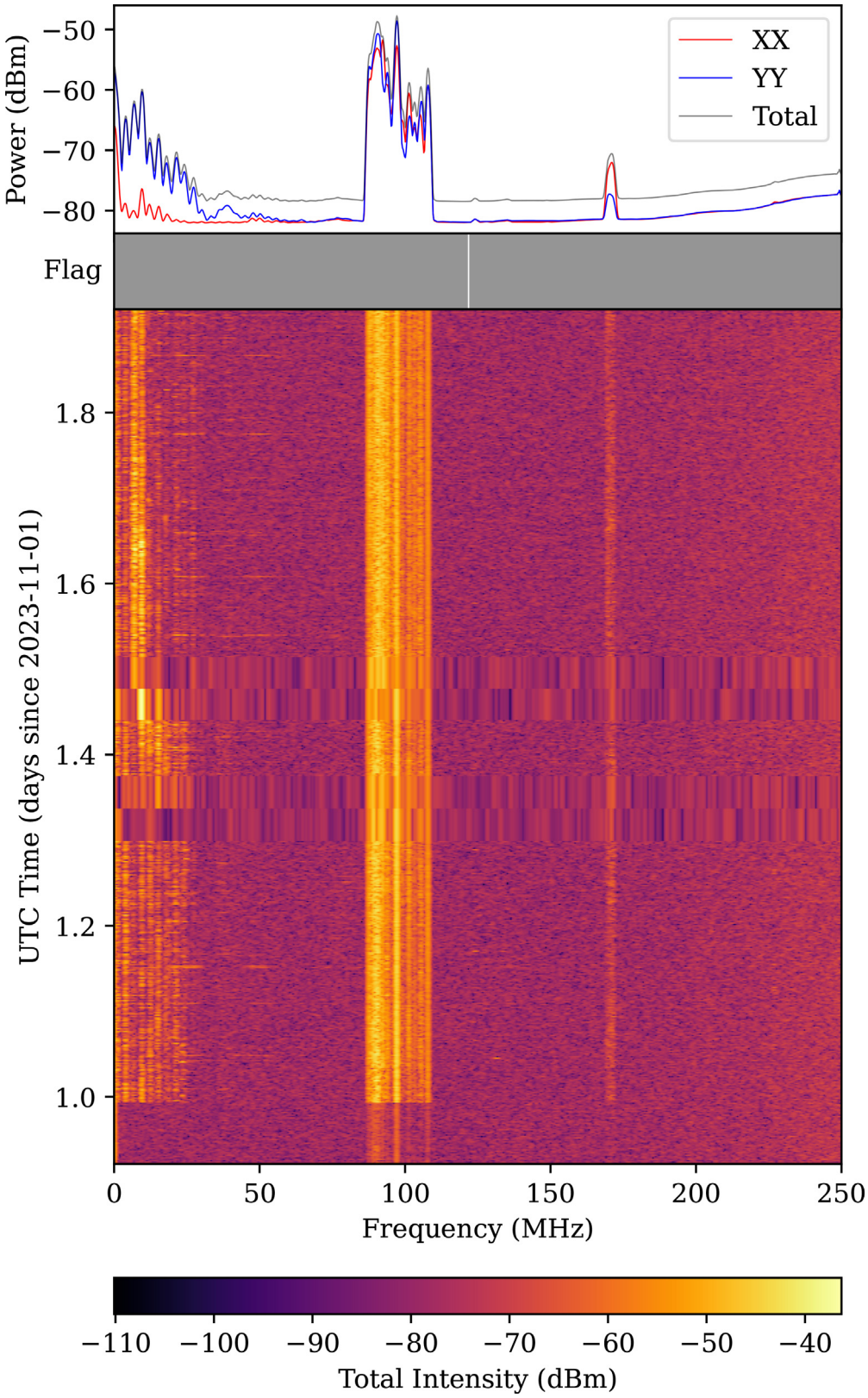


Fig. 4. Overall result plot for UM data. The top panel shows the time-averaged power spectra for both linear polarizations and the total intensity, the middle panel shows the SK flags (gray lines denote the flagged frequencies), and the bottom panel shows a waterfall plot of the total intensity for the entire observation period.

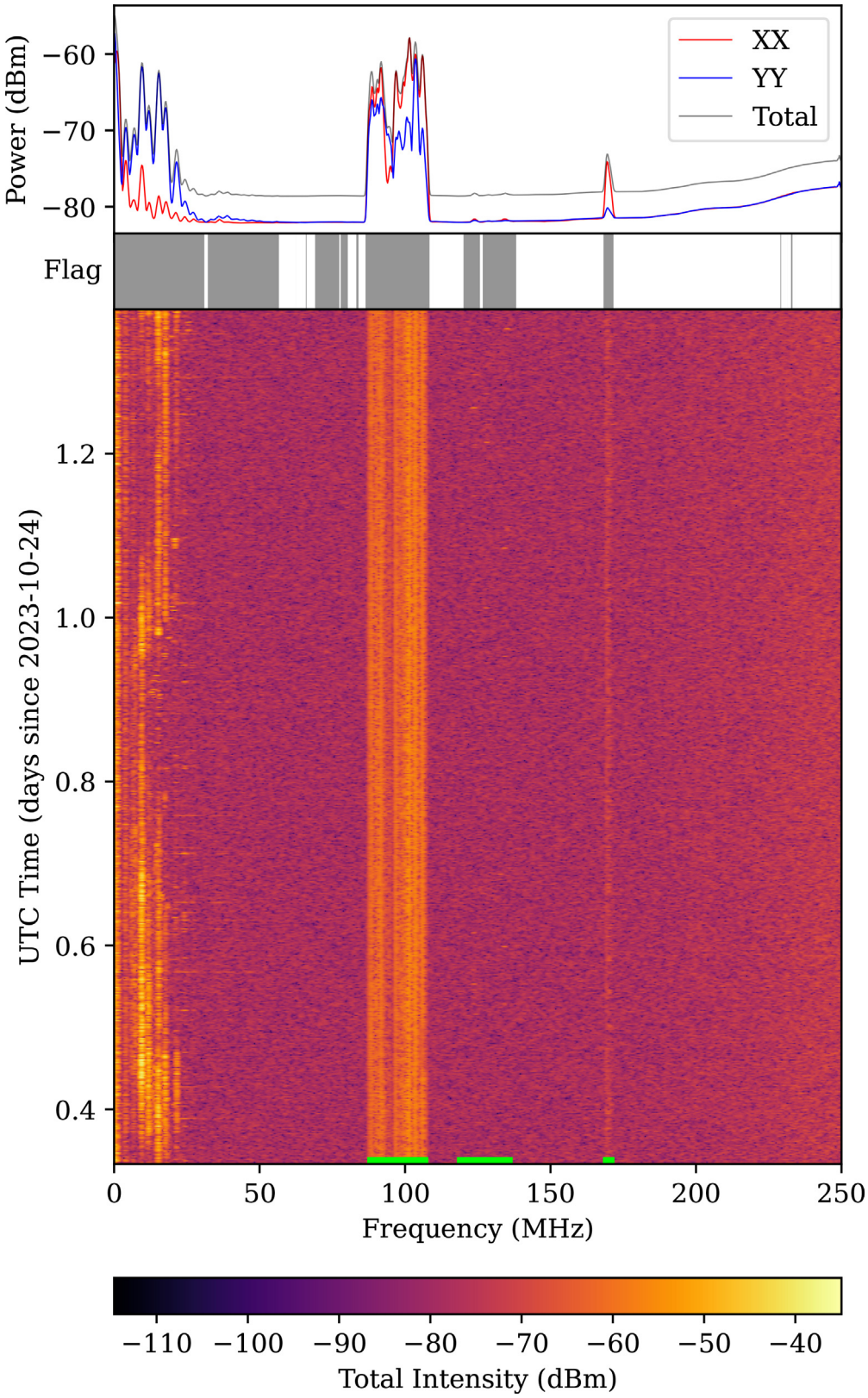


Fig. 5. Similar plot to Fig. 4 but for GL data. The green markers at the bottom of the waterfall plot depicts the three particular groups of narrowband RFI detected; (from left to right) FM analogue radio broadcast (87–108 MHz), aeronautical mobile or airband (117.825–137 MHz), and Malaysian Government mobile services (162.0375–174 MHz).

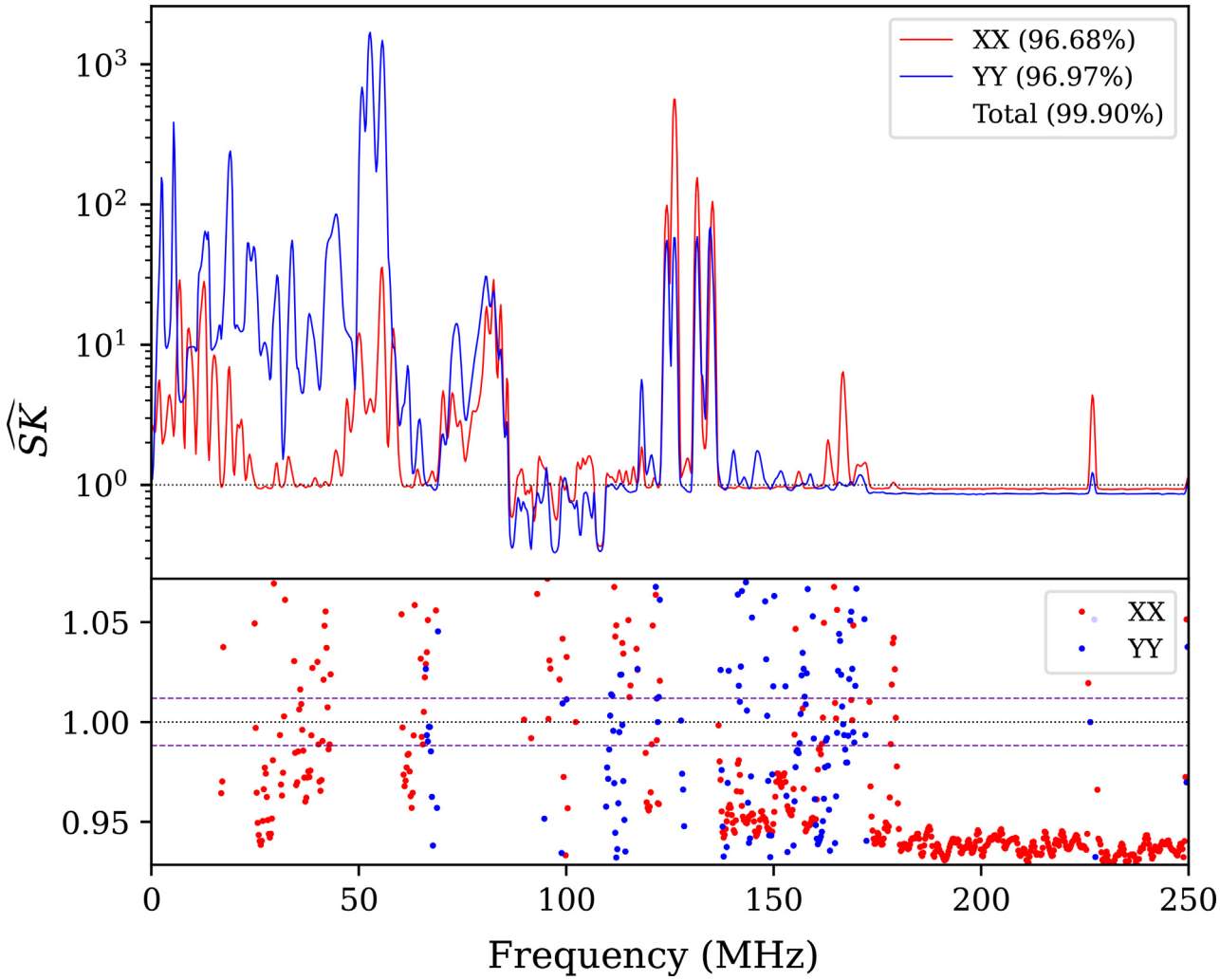


Fig. 6. SK spectra in both linear polarizations for UM data. The top panels show the entire range of SK values while the bottom panels show SK values within the vicinity of the respective SK lower and upper bounds. The percentages associated to each polarization (written in the legend) corresponds to their respective flagging fractions.

frequency channels flagged using the modified SK (shown as grey bars). Figs. 6 and 7 show the SK spectra for UM and GL data respectively. For the UM data, 1022 channels out of 1023 channels (99.90%) are flagged, whereas for the GL data, 469 channels out of 1023 channels (45.85%) are flagged.

Table 4 shows the power ranges of the averaged spectra, while Table 5 shows the summary for SK statistics, both for UM and GL data. The averaged power spectra range and statistics (minimum, maximum, mean, standard deviation, and median) in the UM data consistently surpasses that of the GL data across all cases, with the median SK values for the UM data in both polarizations also exceeding those of the GL data.

These results indicate a higher baseline in the power spectrum and a larger degree of RFI contamination in urban areas, as represented by UM, compared to rural areas, represented by GL. This similar to the results of Umar et al. (2013); Abidin et al. (2021) where RFI levels were seen to depend strongly on population density, primarily attributed to the presence of more telecommunication and broadcasting stations. However, this was previously reported to occur at higher frequencies (e.g. near 1000 and 1800 MHz; Abidin et al., 2009), and our results demonstrate that it does affect the LF - VHF range as well.

In RFI-dominated spectra, the SK shape factor becomes biased, increasing false positive flags (Nita et al., 2016a), which may have been the case for the UM data. Nonetheless, several other factors can physically explain the near-complete RFI contamination in urban environments. Strong narrowband signals can leak into adjacent channels during digitization, leading to overflagging by spectral kurtosis (Smith et al., 2022). Densely packed emitters and poorly tuned devices produce overlapping sidebands that mimic broadband interference. Transient emissions from electronic systems and intermodulation from non-linear components further add to the noise. Additionally, urban reflections and multipath propagation broaden and intensify RFI signatures (Parsons and Gardiner, 1989). Combined, these

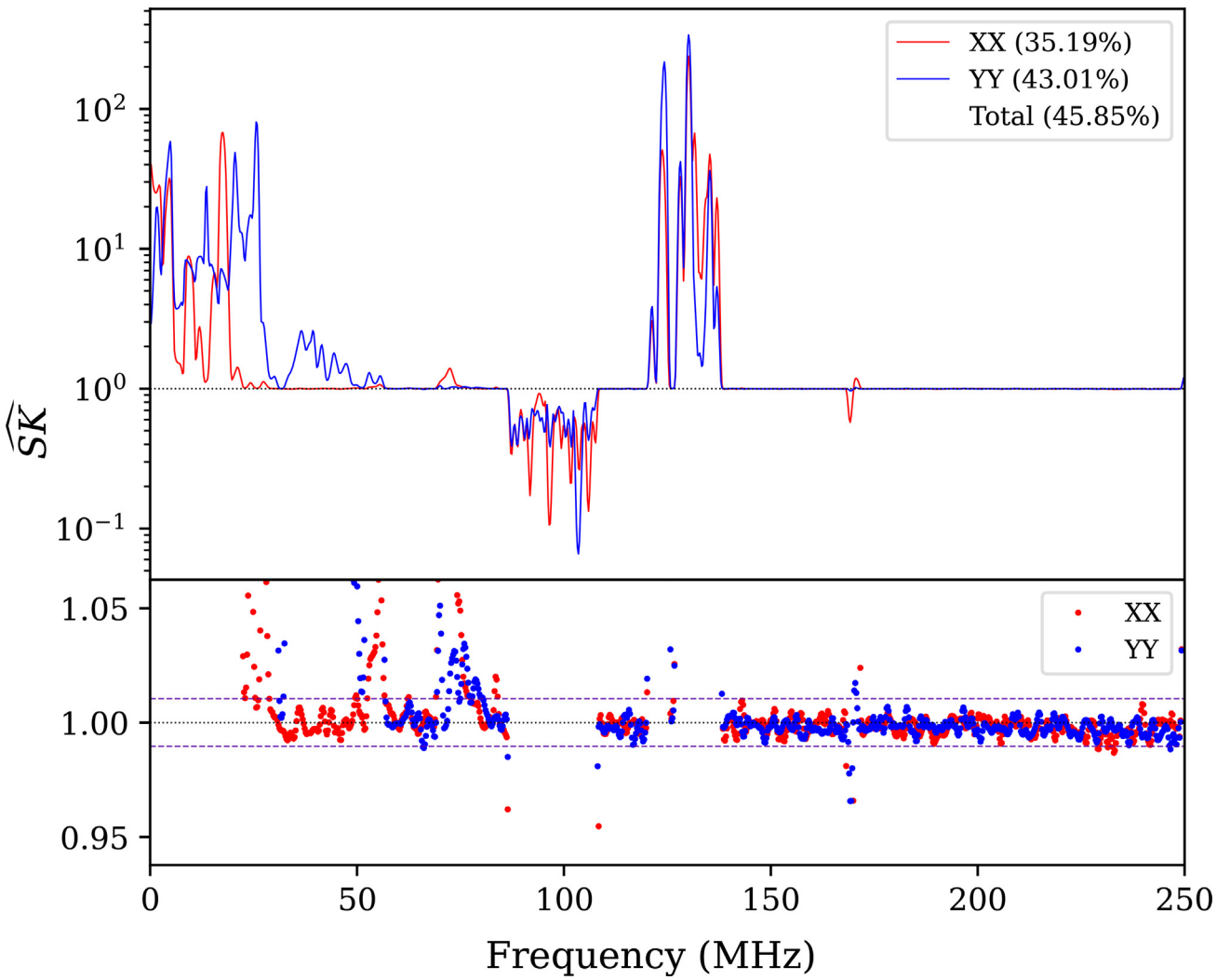


Fig. 7. Similar plot to Fig. 6 .but for GL data.

Table 4
Averaged power spectra range and basic statistics in the UM and GL data. All values are in dBm.

| Statistic | UM | | | GL | | |
|---|---|---|---|---|---|---|
| | XX | YY | Total | XX | YY | Total |
| Minimum | −82.0518 | −81.9125 | −114.7707 | −82.1486 | −82.0870 | −114.7737 |
| Maximum | −51.7386 | −48.5810 | −24.0870 | −57.8832 | −57.3436 | −24.5401 |
| Mean | −78.8963 | −77.6990 | −74.5701 | −79.4308 | −79.0911 | −75.6161 |
| Std. Dev. | 6.1742 | 6.8550 | 7.8493 | 4.9507 | 4.6944 | 6.2942 |
| Median | −81.4583 | −80.8075 | −76.1759 | −81.5000 | −81.4369 | −76.5144 |

effects make narrowband sources appear as continuous interference, especially in densely populated areas.

### 5.2. Spectrum allocation

As the UM spectrum is flagged in almost all frequency channels, only the GL spectrum is used to characterize specific RFI sources. However, it is noteworthy to mention that both the UM and GL data possess the same RFI-channel signature. There are two general types of RFI detected in the data: persistent RFI (with duty cycles of $\gtrsim 50\%$) and transient RFI (with duty cycles of $\lesssim 50\%$). The three persistent RFI signals detected in the data are from 0 to 31.25 MHz, between 86.43 and 108.40 MHz, and between 168.21 and 171.63 MHz (hereinafter referred to as RFI-P1, RFI-P2, and RFI-P3 respectively), while the two transient RFI signals detected in the data are between 32.23 and 56.64 MHz, and between 120.12 and

Table 5
Summarized SK statistics for UM and GL data in both linear polarizations. $\hat{\mu}$ is the median $\widehat{SK}$ value, $d$ is the shape factor, $\delta$ are the upper and lower $\widehat{SK}$ thresholds, and $N$ are the flagged channel counts (and fractions).

| Statistic | UM | | GL | |
|---|---|---|---|---|
| | XX | YY | XX | YY |
| $\hat{\mu}$ | 1.079763 | 1.171981 | 1.013884 | 1.013477 |
| $d$ | 0.926057 | 0.853112 | 0.986293 | 0.986690 |
| $\delta_{\text{lower}}$ | 0.988417 | 0.988168 | 0.989680 | 0.989682 |
| $\delta_{\text{upper}}$ | 1.011790 | 1.012054 | 1.010480 | 1.010479 |
| $N_{\text{lower}}$ | 493 (48.19%) | 492 (48.09%) | 105 (10.26%) | 97 (9.48%) |
| $N_{\text{upper}}$ | 496 (48.48%) | 500 (48.88%) | 255 (24.93%) | 343 (33.53%) |
| $N_{\text{subtotal}}$ | 989 (96.67%) | 992 (96.97%) | 360 (35.19%) | 440 (43.01%) |
| $N_{\text{total}}$ | 1022 (99.90%) | | 469 (45.85%) | |

138.18 MHz (hereinafter referred to as RFI-T1 and RFI-T2 respectively). Any spectrum allocations mentioned are based on the ITU and the Malaysian Communications and Multimedia Commission (MCMC) based on the 2022 Spectrum Allocation document (Malaysian Communications and Multimedia Commission, 2022).

#### 5.2.1. Persistent RFI with diurnal variation

RFI-P1 (0 to 31.25 MHz), shown in Fig. 8, has a unique structure consisting of two distinct emission patterns; a group with relatively consistent emission below 5 MHz and a group of signals with temporally varying amplitudes peaking at −24.54 dBm. Hereinafter, the groups are referred to as RFI-P1a and RFI-P1b respectively. The entire LF – HF range is allocated for all types of operations including mobile services, broadcasting, maritime communications, and amateur use. However, the relatively wide channel spacing in our observation means that these narrow-band emissions are averaged in each frequency bin, retaining only large-scale patterns.

At such low frequencies, RF1-P1a should consist of signals from local and regional radio sources propagating directly or via ground-reflected waves to the data acquisition locations (Hufford, 1952; Hill, 1982; DeMinco, 2000). This is reinforced with the consistency in the signal throughout the entire observation period, which can be attributed to the maximal propagation effects at this frequency range.

In contrast, RF1-P1b has a distinct signature in which the amplitudes in different channels varies with a diurnal pattern in the data as shown in Fig. 9. The frequency at which the brightest emission is observed at a certain time correlates linearly with the solar altitude with a correlation coefficient of 0.9392 as shown in the inset of Fig. 9. This diurnal variation in the peak frequency can be explained by skywave propagation of radio signals in the ionosphere, and is usually prevalent at frequencies below 35 MHz (Wagner et al., 1995; Zhou and Ju, 2019).

In daylight, Lyman-α and X-ray solar radiation enhances the formation of the ionospheric D layer, increasing the ionosphere's opacity of low-frequency signals (Rumi, 1960; Bibl et al., 1961). This enables higher frequencies to pass through the D layer and reflect off the ionospheric F layers. During the night, with no solar radiation, the D layer significantly thins (remaining due to cosmic rays), facilitating more efficient skywave propagation of low-frequency signals. Small scale disturbances in the trend may be solar-induced e.g. solar X-ray flares enhancing D layer photoionization (Thomson and Clilverd, 2001; Kumar and Kumar, 2018; Rozhnoi et al., 2019; Briand et al., 2022; Shamsuddin and Shariff, 2022; Gu et al., 2023) and/or of atmospheric origin e.g. thunderstorms causing atmospheric gravity waves (AGWs) and lightning-induced quasi-electrostatic fields which can disrupt the D layer (Cheng et al., 2007; Lay and Shao, 2011; Shao et al., 2012; Redoblado et al., 2022).

#### 5.2.2. Other Persistent RFI

RFI-P2 (86.43 to 108.40 MHz) exhibits two primary signal groups, delineated by a dip at 95 MHz. While the signal does feature smaller subband divisions, its temporal consistency is evident, with a maximum amplitude of −51.63 dBm. These bands are allocated to mobile services and broadcasting by the ITU (87–108 MHz for Region 3) and MCMC, but is mainly occupied by frequency modulation (FM) analogue radio broadcast. This RFI signal was previously seen in RFI monitoring in the same locations (Abidin et al., 2011; Abidin et al., 2021), and is consistent with monitoring performed in other locations in Malaysia (Umar et al., 2015) as well as in neighbouring countries e.g. Thailand and Indonesia (Hidayat et al., 2014; Jaroenjittichai et al., 2017).

RFI-P3 (168.21 to 171.63 MHz) displays a distinctive single-band signature with a peak amplitude of −59.08 dBm. This signal falls within the mobile services allocation by the ITU (162.0375–174 MHz in all regions), with the 169 to 173.50 MHz range allocated to the Malaysian Government (MLA14).

#### 5.2.3. Transient RFI

RFI-T1 (32.23 to 56.64 MHz) is marked by random emissions dispersed in both time and frequency, reaching a peak intensity of −51.23 dBm. This frequency band has diverse allocations, encompassing mobile services, radiolocation, broadcasting, amateur operations, space research, and radio astronomy. Notably, the 5.149 ITU radio astronomy footnote designates protection for the 37.5 to 38.25 MHz band, specifically for Jupiter's decametric radiation observations. This serves as a reminder to conduct thorough RFI assessments even during observations within radio astronomy-protected bands.

RFI-T1 (in the UM data) also consists of an interesting RFI signal centred at 50 MHz with a 10 MHz bandwidth as shown in Fig. 10, attributed to a newly-used VHF digital communication radio which was previously unseen. Typically, signals within this frequency range traverse through the ionosphere and extend into space, making them unsuitable for skywave propagation of communication signals.

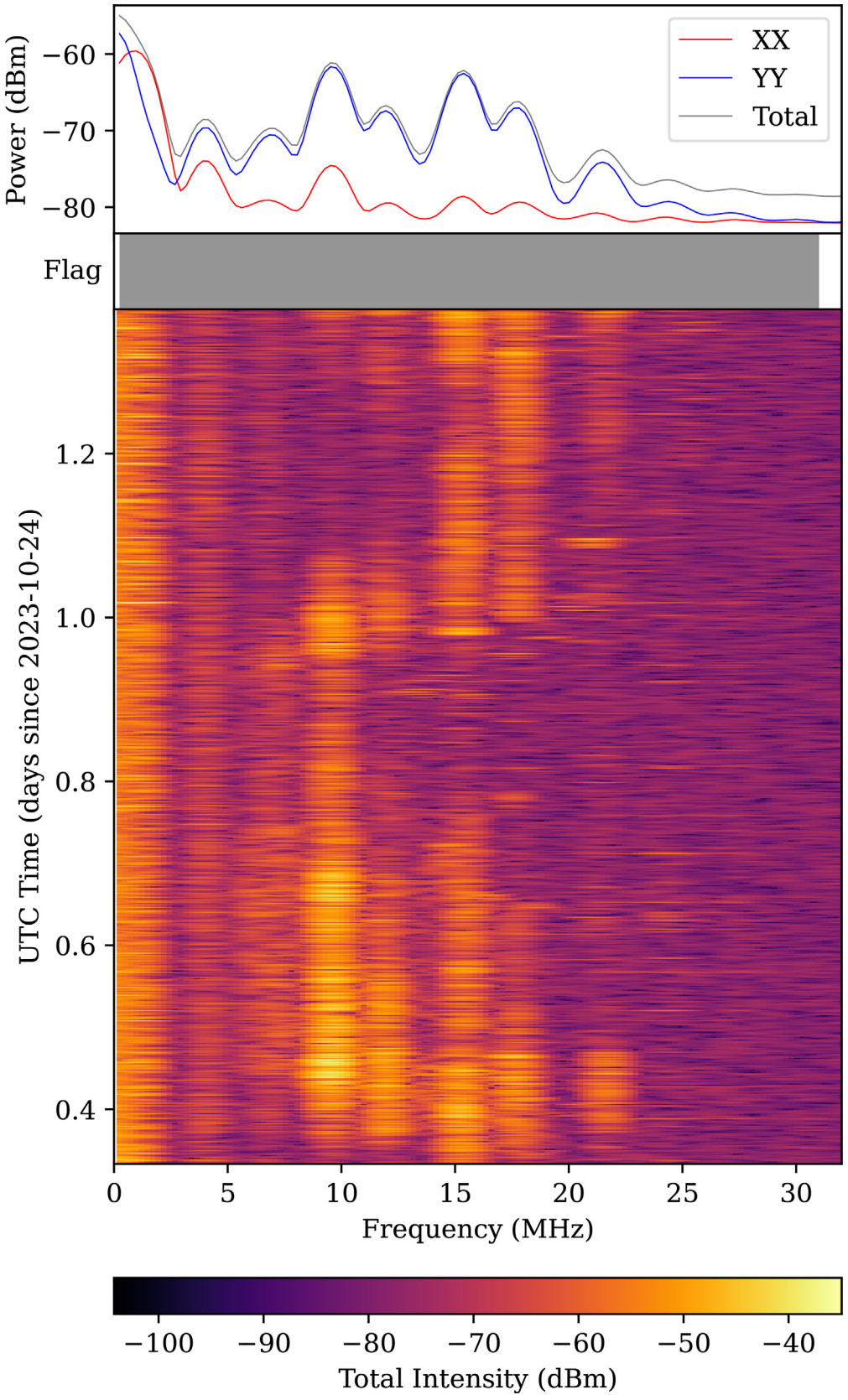


Fig. 8. Similar plot to Fig. 4 but for GL data zoomed into the RFI-P1 .frequency range.

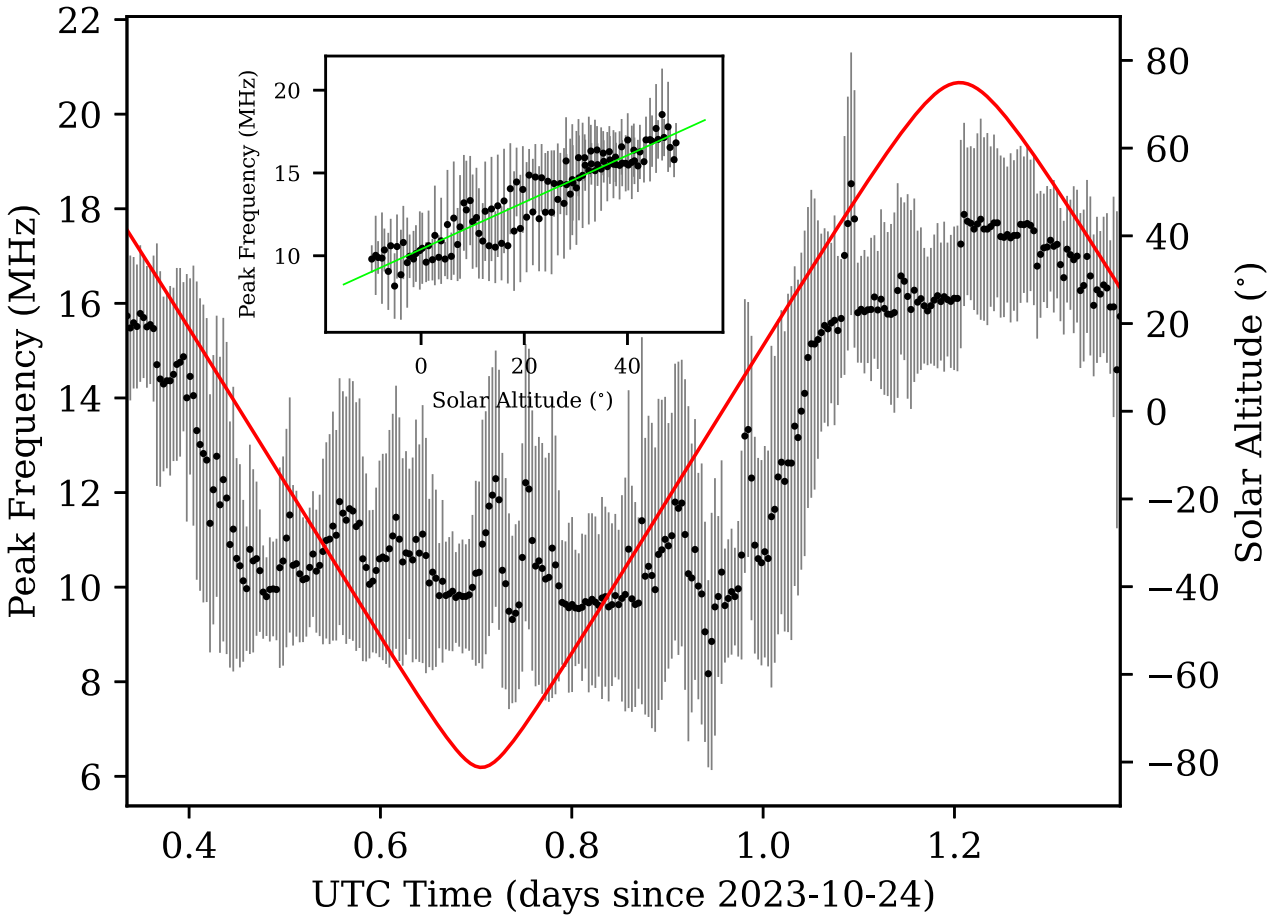


Fig. 9. Summary plot of the diurnal pattern in RF1-P1b of the GL data. The main plot shows the evolution of the peak emission frequency for emissions between 0 and 31.25 MHz, with the black markers and grey error bars representing binned data over every 5-min interval with their $1\sigma$ respectively, and the red line representing the solar altitude. The inset shows the correlation fit between the peak emission frequency in the GL data and the solar attitude, with the green line representing a linear fit to the data. Note that only the data for solar altitudes between $-10^{\circ}$ and $50^{\circ}$ are considered for the fitting due to the constant darkness from dusk to dawn and the saturation of the formation of the ionospheric D layer near noon.

However, equatorial ionospheric anomalies (EIA) can augment the reflection of such radio signals (Stening, 1992; Lin et al., 2007; Ram et al., 2009; Balan et al., 2018). Interaction between the equatorial daytime electric field and the geomagnetic field drifts the ionospheric plasma upward and away from the dip equator, resulting in a double-peak structure in the plasma density in the north–south direction. In this case, according to a geomagnetic reference frame, the southern hump in the EIA can be seen passing over Malaysia when the emissions are prevalent as shown in Fig. 11.

Similar to RFI-T1, RFI-T2 (120.12 to 138.18 MHz) exhibits random signals, featuring a higher maximum intensity of −43.23 dBm. This frequency range is designated for aeronautical mobile services or airband, specifically within the 117.825 to 137 MHz range allocated by the ITU for all regions, where amplitude modulation voice transmissions (VHF-AM) facilitate communication between aircraft and ground stations, commonly referred to as air traffic control (ATC) services (Federal Aviation Administration, 1992). Under footNote 5.200, ITU also allocates the 121.5 and 123.1 MHz frequencies for aeronautical emergency communications, primarily handling distress and safety calls.

## 6. RFI mitigation methods

To continue performing radio observations in environments with high RFI contamination (either due to high population densities such as in Malaysia, and/or due to spectrum allocated to other uses), RFI mitigation techniques have to be implemented. Various mitigation methods can be considered, each with varying complexity and reliability (Fridman and Baan, 2001). Here we test out two post-observation mitigation methods i.e. removal of RFI corrupted data after data collection, and one physical RFI suppression method, as well as discuss other possible mitigation procedures.

### 6.1. Post-observation RFI mitigation

Post-observation RFI mitigation in radio astronomy is highly advantageous due to its versatility, allowing for adjustable flagging thresholds and parameters tailored to

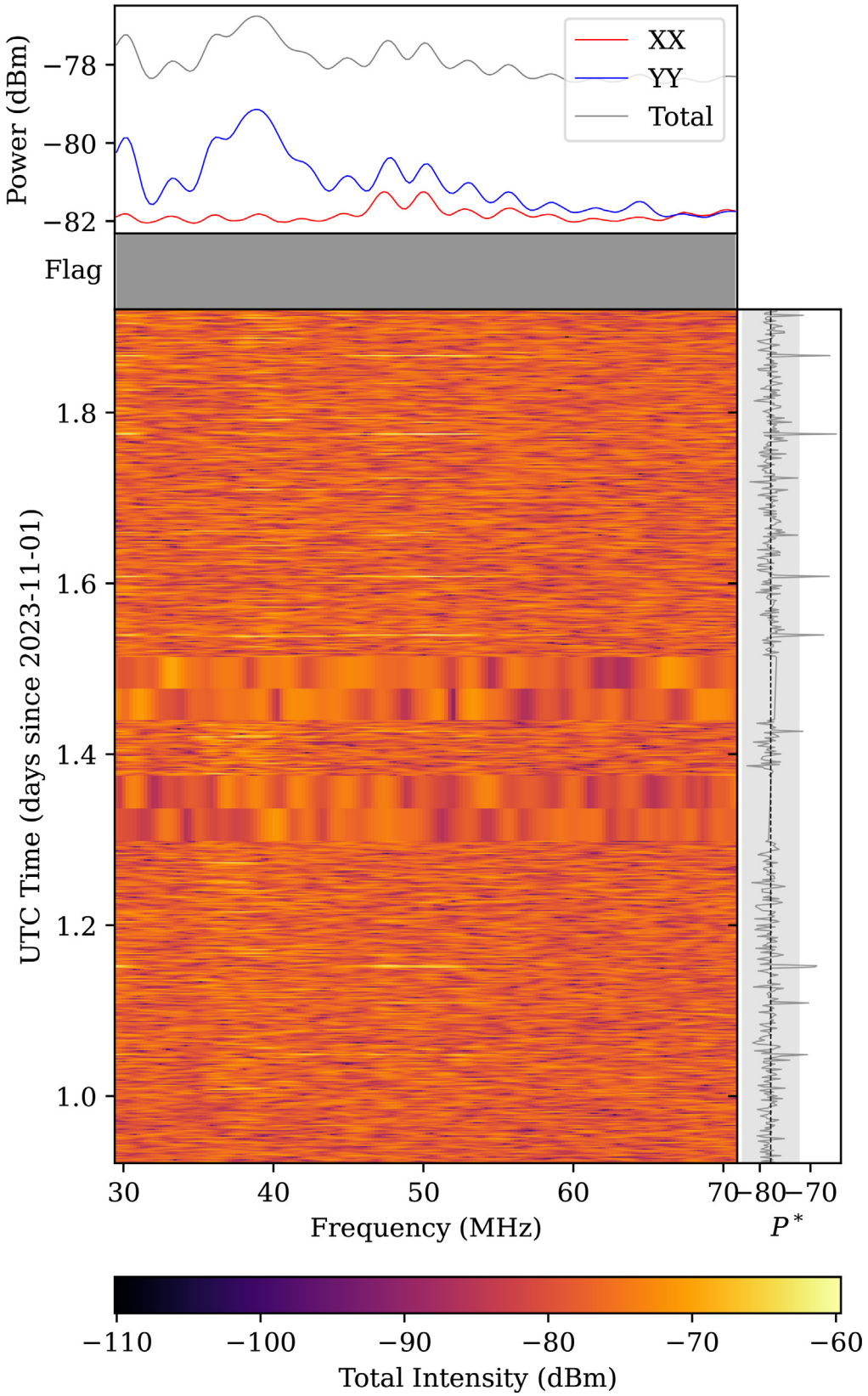


Fig. 10. Similar plot to Fig. 4 but zoomed into the RFI-T1 frequency range. The subplot to the right of the waterfall plot illustrates the temporal evolution of RFI-T1 within the 45 – 55 MHz range. The grey line, black dashed line, and shaded light grey region indicate the averaged power spectrum $P^*$, the mean power, and the corresponding $3\sigma$ confidence levels respectively, all within the said .frequency range.

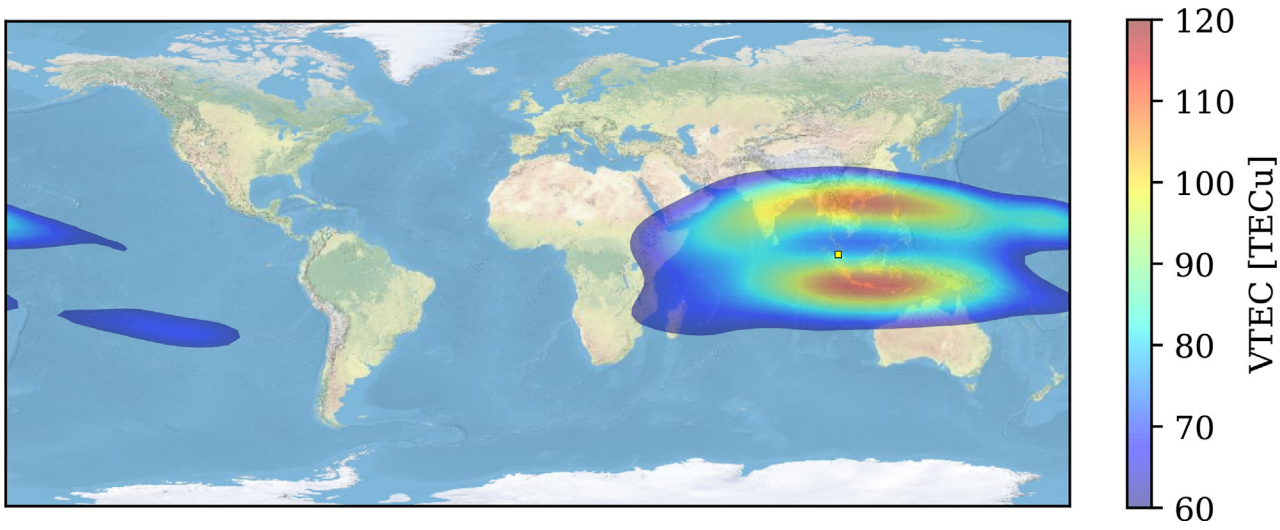


Fig. 11. Vertical Total Electron Content (VTEC) map at 15:30 p.m. (GMT + 8) on 2 November 2023 from the Chinese Academy of Sciences' real-time global ionospheric map (CAS RT-GIM) model as described in Li et al. (2020). The yellow square marks the location of. the UM station.

the target data quality, all while having minimal to no effect on the instrument's front- and back-end systems.

One of the mitigation methods is the Median Absolute Deviation (MAD) filter which utilizes high-order statistics. MAD considers that RFI signals are simply outliers of random Gaussian noise, but utilizes the median deviation instead of the standard deviation which can be influenced by outliers (Buch et al., 2016). MAD can be applied to either the time or frequency domain, but suffers if the RFI contaminates more that 50% of the data. When applied to UM and GL data in both domains, strong and transient RFI can be seen to mitigated effectively. However, weak and persistent RFI signals, especially in the vicinity of stronger RFI are often left unflagged. Shown in Fig. 12 and Table 6 is the result of the application of the MAD filter on the GL data.

Another post-observation RFI mitigation method is autocleaning where the RFI waveform is estimated and subtracted from the data. The RFI waveform can be estimated using various filtering techniques including spline-smoothing, wavelet analysis, Wiener filtering, and parametric estimation (Baan, 2019). One of which is the discrete wavelet transform (DWT), and this has been shown to be effective in suppressing various types of RFI (Camps and Tarongí, 2009; Díez-García and Camps, 2019; Tian-qi et al., 2021). When a 3-level Haar DWT is applied to both UM and GL data, all persistent RFIs were detected well, but in certain cases, the RFI are either undercorrected (e.g. RFI-P3) or overcompensated (RFI-P2) as shown in Fig. 12. Notably, the gradual positive slope in the signals above 200 MHz was falsely suppressed, posing a threat to data with an uncorrected bandpass shape or a smooth continuum background emission. Table 6 shows the statistics of the DWT performed on the GL data.

In recent years, machine learning (ML) has become a powerful tool in astronomy. Techniques such as convolutional neural networks (CNNs), deep fully convolutional networks (DFCNs), and autoencoders have shown the ability to efficiently identify and remove RFI from both simulated and real radio data (Kerrigan et al., 2019; Yang et al., 2020; Toit et al., 2024). Supervised ML models trained on labelled data are particularly effective and fast, while unsupervised approaches, which leverage large datasets, offer more robust detection of unknown RFI patterns (Ghanney and Ajib, 2020). ML models can also be trained exclusively on clean, uncontaminated data, allowing them to distinguish RFI from all known astronomical signals and system noise (Mesarcik et al., 2022).

### 6.2. Physical RFI suppression

Physical methods are also viable in suppressing RFI, with the main advantages of real-time application and the usability of the suppressed signals.

One of them is using frequency filters which uses priori RFI information to attenuate signals in the contaminated frequency ranges directly from the antenna. The simplest of which is a band stop filter created based on extensive RFI monitoring. Based on our results, we synthesized a band stop filter with a 50 dB attenuation and a roll range between 76 and 122 MHz, and it was able to suppress RFI-P2 in a short RFI monitoring test performed at UM as shown in Fig. 13. However, traditional filtering techniques are spectrally inefficient due to their gradual roll-off characteristics, and while superconducting filters offer much sharper selectivity, they are considerably more expensive. Moreover, the performance of band stop filters depend highly on the quality of the RFI monitoring, and is unable to mitigate transients. To deal with time-varying RFI, adaptive filters which constantly estimate and filter RFI signals within a closed loop (Widrow and Stearns, 1985) can be implemented, and has been seen to

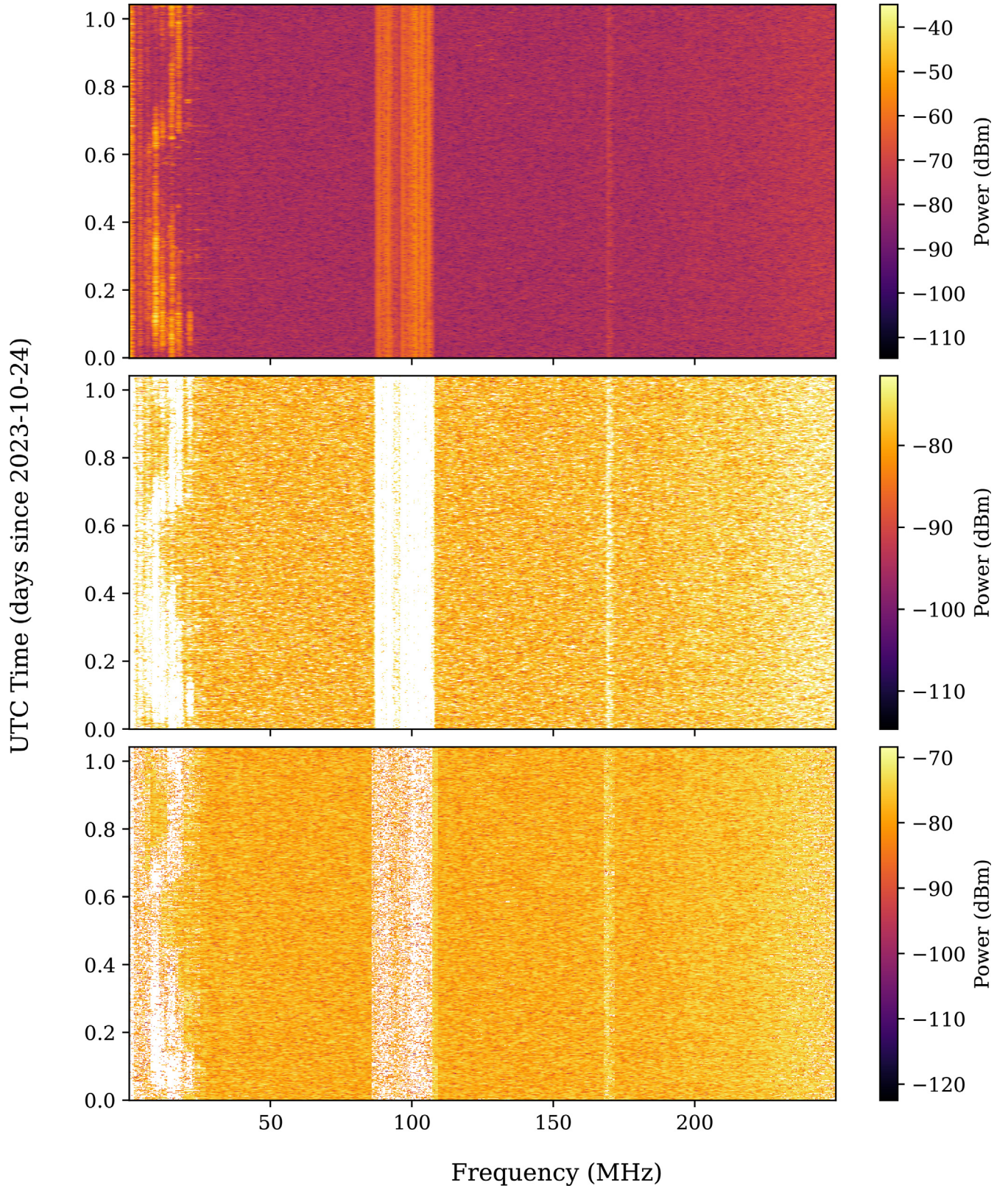


Fig. 12. Waterfall plot of the GL data before any RFI mitigation (top panel), after applying the MAD filter (middle panel), and after applying the DWT filter (bottom panel). White pixels denote the time and frequency at which the data has been flagged.

Table 6
Averaged power spectra range in the GL data before any mitigation, and after mitigation using MAD filter and DWT. All values are in dBm.

| Type | Original | MAD filter | DWT |
|---|---|---|---|
| Minimum | −114.7737 | −114.7737 | −235.4863 |
| Maximum | −24.5401 | −71.0455 | −68.0387 |
| Mean | −75.6161 | −78.4810 | −77.8272 |
| Std. Dev. | 6.2942 | 3.3162 | 3.9416 |
| Median | −76.5144 | −77.9297 | −77.3657 |

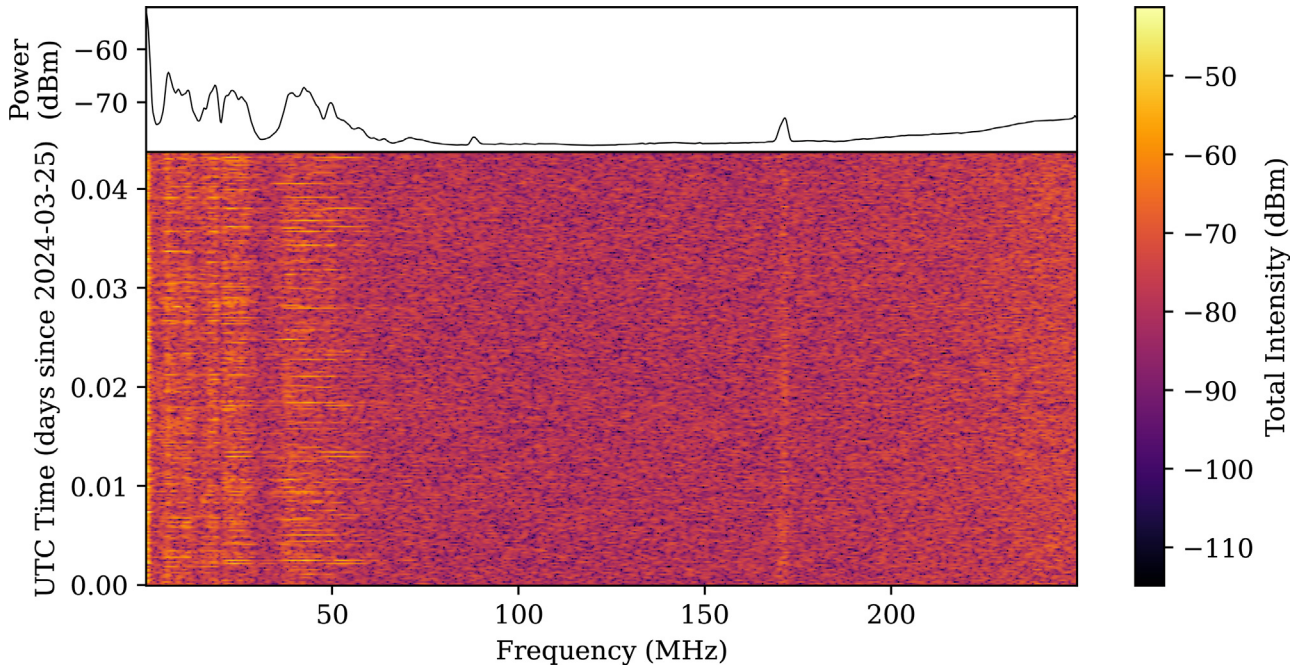


Fig. 13. Waterfall plot of a short RFI monitoring test performed at UM using the band stop filter targeted on RFI-P2.

be effective on various radio telescopes (e.g. Finger et al., 2017).

Another type of physical suppression involves spatial-filtering which performs adaptive suppression of RFI signals based on their direction-of-arrival (DOA), as applied in radar and communication systems (Kocz et al., 2010; Steeb et al., 2016). However, this method in its simplest requires an auxiliary reference antenna or multi-feed receivers to capture the RFI DOA, which can only be used to overcome single strong interferers and is therefore unusable in complex RFI environments.

To extend that, cross-correlation data when performing VLBI between telescopes with large baselines is relatively free from local RFI as it emulates the spatial filtering technique. Only signals present in all telescopes – either from astronomical sources or far-field interference – would survive the correlation process. Ultimately, combining spatial suppression and post-observation mitigation techniques will be able to give the best outcome in terms of RFI mitigation (Nita and Hellbourg, 2020).

Although our results are based on post-detection processing, it is necessary to acknowledge the benefits of real-time RFI suppression at the intermediate frequency (IF) stage. Strong and narrowband RFI signals can cause spectral leakage, contaminating neighbouring channels even after offline mitigation. Implementing online IF baseband clipping prior to digitalization has been shown to be highly effective in removing such signals at their source (see Fridman and Baan, 2001). Unfortunately, our instrument setup does not support real-time IF-domain blanking; however, future implementations incorporating FGPS-based backends may offer a promising solution (e.g. Quirós-Olozábal et al., 2016).

## 7. Conclusion

We report the measurements of low frequency RFI in two locations in Malaysia; UM representing an urban environment, and GL representing a candidate RNZ. We detected higher levels of RFI in UM than in GL in this fre-

Table 7
Summary of low to very high frequency RFI detected using modified GSK in this paper.

| RFI Type | Identifier | Frequency Range (MHz) | Max. Power (dBm) | Spectrum Allocation | Notes |
|---|---|---|---|---|---|
| Persistent | RFI-P1 | 0.00 – 31.25 | −24.54 | Mobile services, broadcasting, maritime, amateur | Constant direct/ground-wave propagation (RFI-P1a) and skywave propagation with diurnal pattern (RFI-P1b) |
| | RFI-P2 | 86.43 – 108.40 | −51.63 | Mobile services, broadcasting | FM analogue radio broadcast |
| | RFI-P3 | 168.21 – 171.63 | −59.08 | Mobile services | Allocated to Malaysian Government (MLA14) |
| Transient | RFI-T1 | 32.23 – 56.64 | −51.23 | Mobile services, radiolocation, broadcasting, amateur, space research, radio astronomy | Detection of new VHF signal augmented by EIA skywave propagation |
| | RFI-T2 | 120.12 – 138.18 | −43.23 | Aeronautical mobile services | Air traffic control VHF-AM |

quency range. Using modified GSK, we were able to characterize three groups of persistent RFI and two groups of transient RFI, each attributed to their respective ITU and MCMC spectrum allocations. Some of the RFI detected also exhibit variabilities corresponding to natural phenomena e.g. diurnal frequency evolution due to skywave propagation, and augmentation of skywave propagation by EIA. Shown in Table 7 is a summary of all the RFI groups detected and their properties.

Various post-observation RFI mitigation and physical RFI suppression techniques were tested on our data as well, and were effective in removing a significant amount of RFI. Ultimately, by combining RNZ characteristics and these mitigation techniques, GL is appropriately capable for relatively low frequency radio astronomy for diffuse radio observations, deep extragalactic surveys, pulsar and FRB monitoring, and solar observations.

This research can also be viewed as a continuation of the previous RFI monitoring efforts in Malaysia (especially Abidin et al., 2021), step towards the preparation for the development of a research-grade radio telescope in Malaysia. It should be noted that the results in this study are based on a single day of observations at each site. While this duration was sufficient to identify key RFI sources and examine short-term patterns such as diurnal variations, it does not capture longer-term or seasonal trends. Therefore, our future works will therefore include longer monitoring sessions to capture the full range of RFI variability, as well as a larger number of monitoring stations with a sparse spatial distribution to compare a wider range of environmental variability and population differences.

## Declaration of Competing Interest

The authors declare that they have no known competing financial interests or personal relationships that could have appeared to influence the work reported in this paper.

## Acknowledgments

We acknowledge the support provided by Malaysia's Ministry of Science, Technology and Innovation (MOSTI) under the Technology Development Fund (TDF07221598). We were also supported by the People's Republic of China's Ministry of Science and Technology (MOST) under the National Key R&D Programme (SQ2022YFE010485). We finally acknowledge the Chinese Academy of Sciences under the International Partnership Program of the Bureau of International Cooperation of the Chinese Academy of Science and Technology: "Belt and Road" Project (114A11KYSB20200001).

We would like to express our sincere gratitude to the National Astronomical Observatories (NAOC) and Yunnan Astronomical Observatory (YNAO) of the Chinese Academy of Sciences for providing us with the equipments and technical support. We thank the members of the Radio Cosmology Research Laboratory, Universiti Malaya, and the staffs of the Glami Lemi Biotechnology Research Centre, Jelebu, who were involved in the data collection phase of the project. The work in this article is also part of the efforts by the Radio Astronomy Frequency Committee of Malaysia (RAFCOM), which monitors the radio astronomical RFI in Malaysia.

We greatly appreciate Prof. Gelu M. Nita from the Center for Solar-Terrestrial Research at the New Jersey Institute of Technology for his invaluable guidance on the details of the GSK method. We also thank Raúl Díez García from the Universitat Politécnica de Catalunya for his assistance on the DWT RFI mitigation method. Finally, we gratefully acknowledge the anonymous reviewers for their insightful comments and suggestions, which significantly improved the quality of this article.

## References

Abidin, Z.Z., Bahari Ramadzan Syed Adnan, S., Ibrahim, Z.A., 2010. Rfi profiles of prime candidate sites for the first radio astronomical telescope in Malaysia. New Astron. 15 (3), 307–312. https://doi.org/10.1016/j.newast.2009.09.003.

Abidin, Z.Z., Ibrahim, Z.A., Adnan, S.B.R.S., et al., 2009. Investigation of radio astronomical windows between 1mhz and 2060mhz in universiti malaya, Malaysia. New Astron. 14 (6), 579–583. https://doi.org/10.1016/j.newast.2009.02.003.

Abidin, Z.Z., Ibrahim, Z.A., Rosli, Z., et al., 2011. Methods and applications of radio frequency interference surveys for radio astronomy in malaysia. In: Proceeding of the 2011 IEEE International

Conference on Space Science and Communication (IconSpace). IEEE. https://doi.org/10.1109/iconspace.2011.6015878.
Abidin, Z.Z., Ibrahim, Z.A., Rosli, Z., et al., 2012. An rfi investigation for setting up a vlbi station below 2.8 ghz in malaysia. New Astron. 17 (2), 61–64. https://doi.org/10.1016/j.newast.2011.06.001.
Abidin, Z.Z., Rosli, Z., Radzi, M.S.M., et al., 2021. Radio quiet and radio notification zones characteristics for radio astronomy in medium densely populated areas and humid tropical countries. J. Astron. Telescopes, Instrum., Syst. 7 (02). https://doi.org/10.1117/1.jatis.7.2.027001.
Abidin, Z.Z., Umar, R., Ibrahim, Z.A., et al., 2013. Investigation on the frequency allocation for radio astronomy at the L band. Publ. Astron. Soc. Austral. 30. https://doi.org/10.1017/pasa.2013.25.
Baan, W.A., 2019. Implementing RFI mitigation in radio science. J. Astron. Instrument. 08 (01). https://doi.org/10.1142/s2251171719400105.
Balan, N., Liu, L., & Le, H. (2018). A brief review of equatorial ionization anomaly and ionospheric irregularities. Earth and Planetary Physics, 2 (4), 1–19. URL: https://doi.org/10.26464/epp2018025. doi:10.26464/epp2018025.
Bentum, M.J., & Boonstra, A.-J. (2011). Low frequency astronomy — the challenge in a crowded rfi environment. In 2011 XXXth URSI General Assembly and Scientific Symposium (p. 1–4). IEEE volume 40. URL: doi: 10.1109/URSIGASS.2011.6050736. doi:10.1109/ursigass.2011.6050736.
Bibl, K., Paul, A., Rawer, K., 1961. Absorption in the D and E regions and its time variation. J. Atmos. Terr. Phys. 23, 244–259. https://doi.org/10.1016/0021-9169(61)90049-6.
Briand, C., Clilverd, M., Inturi, S., et al., 2022. Role of hard X-ray emission in ionospheric D-layer disturbances during solar flares. Earth, Planets and Space 74 (1). https://doi.org/10.1186/s40623-022-01598-2.
Buch, K.D., Bhatporia, S., Gupta, Y., et al., 2016. Towards real-time impulsive RFI mitigation for radio telescopes. J. Astron. Instrument. 05 (04). https://doi.org/10.1142/s225117171641018x.
Burns, R.A., Uno, Y., Sakai, N., et al., 2023. A keplerian disk with a four-arm spiral birthing an episodically accreting high-mass protostar. Nat. Astron. 7 (5), 557–568. https://doi.org/10.1038/s41550-023-01899-w.
Camps, A., Tarongí, J., 2009. RFI mitigation in microwave radiometry using wavelets. Algorithms 2 (3), 1248–1262. https://doi.org/10.3390/a2031248.
Cheng, Z., Cummer, S.A., Su, H., et al., 2007. Broadband very low frequency measurement of d region ionospheric perturbations caused by lightning electromagnetic pulses. J. Geophys. Res.: Space Phys. 112 (A6). https://doi.org/10.1029/2006ja011840.
DeMinco, N., 2000. Propagation prediction techniques and antenna modeling (150 to 1705 kHz) for intelligent transportation systems (ITS) broadcast applications. IEEE Antennas Propag. Mag. 42 (4), 9–34. https://doi.org/10.1109/74.868050.
Di Vruno, F., Winkel, B., Bassa, C.G., et al., 2023. Unintended electromagnetic radiation from starlink satellites detected with lofar between 110 and 188 mhz. Astron. Astrophys. 676, A75. https://doi.org/10.1051/0004-6361/202346374.
Díez-García, R., Camps, A., 2019. Impact of signal quantization on the performance of RFI mitigation algorithms. Remote Sensing 11 (17), 2023. https://doi.org/10.3390/rs11172023.
Dou, Y., Gary, D.E., Liu, Z., et al., 2009. The Korean Solar Radio Burst Locator (KSRBL). Publ. Astron. Soc. Pac. 121 (879), 512–526. https://doi.org/10.1086/599624.
Du Toit, C.D., Grobler, T.L., Ludick, D.J., 2024. A comparison framework for deep learning rfi detection algorithms. Mon. Not. R. Astron. Soc. 530 (1), 613–629. https://doi.org/10.1093/mnras/stae892.
Federal Aviation Administration (1992). AC 90-50D requirements for 760-channel VHF radio for aeronautical operations. Available at https://www.faa.gov/regulations_policies/advisory_circulars/index.cfm/go/document.information/documentID/23091.
Finger, R., Curotto, F., Fuentes, R., et al., 2017. A FPGA-based fast converging digital adaptive filter for real-time RFI mitigation on ground based radio telescopes. Publ. Astron. Soc. Pac. 130 (984), 025002. https://doi.org/10.1088/1538-3873/aa972f.
Fridman, P.A., Baan, W.A., 2001. RFI mitigation methods in radio astronomy. Astron. Astrophys. 378 (1), 327–344. https://doi.org/10.1051/0004-6361:20011166, URL: https://doi.org/10.1051/0004-6361:20011166.
Ghanney, Y., Ajib, W., 2020. Radio frequency interference detection using deep learning. In: In 2020 IEEE 91st Vehicular Technology Conference (VTC2020-Spring). IEEE. https://doi.org/10.1109/vtc2020-spring48590.2020.9129612.
Gu, X., Yi, J., Wang, S., et al., 2023. Comparison of vlf signal responses to solar flares along daytime and nighttime propagation paths. Remote Sensing 15 (4), 1018. https://doi.org/10.3390/rs15041018.
Gupta, Y., Ajithkumar, B., Kale, H.S. et al. (2017). The upgraded GMRT: Opening new windows on the radio universe. Current Science, 113(04), 707. URL: https://doi.org/10.18520/cs/v113/i04/707-714. doi:10.18520/cs/v113/i04/707-714.
van Haarlem, M.P., Wise, M.W., Gunst, A.W., et al., 2013. LOFAR: The LOw-Frequency ARray. Astron. Astrophys. 556, A2. https://doi.org/10.1051/0004-6361/201220873.
Hamidi, Z.S., Abidin, Z.Z., Ibrahim, Z.A. et al. (2012a). Indication of radio frequency interference (rfi) sources for solar burst monitoring in malaysia. In AIP Conference Proceedings (p. 43–46). AIP. doi:10.1063/1.4730684.
Hamidi, Z.S., Abidin, Z.Z., Ibrahim, Z.A. et al. (2011). Preliminary analysis of investigation radio frequency interference (rfi) profile analysis at universiti teknologi mara. In Proceeding of the 2011 IEEE International Conference on Space Science and Communication (IconSpace) (p. 311–313). IEEE volume 2. doi:10.1109/iconspace.2011.6015907.
Hamidi, Z.S., Abidin, Z.Z., Ibrahim, Z.A., et al., 2012b. Influence factors of radio frequency interference (rfi) for solar radio astronomy purpose at national space centre, Malaysia. Thai J. Phys. 8, 235–238.
Hidayat, T., Munir, A., Dermawan, B., et al., 2014. Radio frequency interference measurements in Indonesia: A survey to establish a radio astronomy observatory. Exp. Astron. 37 (1), 85–108. https://doi.org/10.1007/s10686-013-9369-7.
Hill, D. (1982). HF ground wave propagation over forested and built-up terrain. Inst. for Telecommunication Sciences. National Telecommunications and Information Administration, Boulder, CO.,.
Hufford, G.A., 1952. An integral equation approach to the problem of wave propagation over an irregular surface. Q. Appl. Math. 9 (4), 391–404. https://doi.org/10.1090/qam/44350.
International Telecommunication Union (2013). Handbook on Radio Astronomy. Geneva, Switzerland (R-HDB-22-2013 ed.). Available at https://www.itu.int/pub/R-HDB-22-2013.
International Telecommunication Union (2015). Handbook on National Spectrum Management. Geneva, Switzerland (R-HDB-21-2015 ed.). Available at https://www.itu.int/pub/R-HDB-21-2015.
Jaroenjittichai, P., Punyawarin, S., Singwong, D., et al., 2017. Radio frequency interference site survey for Thai radio telescopes. J. Phys: Conf. Ser. 901, 012062. https://doi.org/10.1088/1742-6596/901/1/012062.
Kassim, N.E., Perley, R.A., Erickson, W.C., et al., 1993. Subarcminute resolution imaging of radio sources at 74 mhz with the very large array. Astron. J. 106, 2218. https://doi.org/10.1086/116795.
Kerrigan, J., Plante, P.L., Kohn, S., et al., 2019. Optimizing sparse rfi prediction using deep learning. Mon. Not. R. Astron. Soc. 488 (2), 2605–2615. https://doi.org/10.1093/mnras/stz1865.
Kocz, J., Briggs, F.H., Reynolds, J., 2010. Radio frequency interference removal through the application of spatial filtering techniques on the parkes multibeam receiver. Astron. J. 140 (6), 2086–2094. https://doi.org/10.1088/0004-6256/140/6/2086.
Kumar, A., Kumar, S., 2018. Solar flare effects on d-region ionosphere using vlf measurements during low- and high-solar activity phases of solar cycle 24. Earth, Planets and Space 70 (1). https://doi.org/10.1186/s40623-018-0794-8.

Labate, M.G., Waterson, M., Alachkar, B., et al., 2022. Highlights of the Square Kilometre Array Low Frequency (SKA-LOW) telescope. Journal of Astronomical Telescopes, Instruments, and Systems 8 (01). https://doi.org/10.1117/1.jatis.8.1.011024.

Lay, E.H., Shao, X.-M., 2011. Multi-station probing of thunderstorm-generated D-layer fluctuations by using time-domain lightning waveforms: multi-station VLF measurement of D-layer. Geophys. Res. Lett. 38 (23). https://doi.org/10.1029/2011gl049790.

Li, Z., Wang, N., Hernández-Pajares, M., et al., 2020. Igs real-time service for global ionospheric total electron content modeling. J. Geodesy 94 (3). https://doi.org/10.1007/s00190-020-01360-0.

Lin, C.H., Liu, J.Y., Fang, T.W., et al., 2007. Motions of the equatorial ionization anomaly crests imaged by FORMOSAT-3/COSMIC. Geophys. Res. Lett. 34 (19). https://doi.org/10.1029/2007gl030741.

Liquid Instuments (2023). Moku:Lab Specifications. San Diego, CA (v23-1028 ed.). Available at https://www.liquidinstruments.com/products/hardware-platforms/mokulab/.

Lonsdale, C., Cappallo, R., Morales, M., et al., 2009. The Murchison Widefield Array: Design overview. Proc. IEEE 97 (8), 1497–1506. https://doi.org/10.1109/jproc.2009.2017564.

Malaysian Communications and Multimedia Commission (2022). Spectrum plan 2022. Available at https://www.mcmc.gov.my/en/spectrum/spectrum-management.

Mesarcik, M., Boonstra, A.-J., Ranguelova, E., et al., 2022. Learning to detect radio frequency interference in radio astronomy without seeing it. Mon. Not. R. Astron. Soc. 516 (4), 5367–5378. https://doi.org/10.1093/mnras/stac2503.

Nita, G.M., Gary, D.E., 2010a. The generalized spectral kurtosis estimator. Month. Not. Roy. Astron. Soc.: Lett. 406 (1), L60–L64. https://doi.org/10.1111/j.1745-3933.2010.00882.x.

Nita, G.M., Gary, D.E., 2010b. Statistics of the spectral kurtosis estimator. Publ. Astron. Soc. Pac. 122 (891), 595–607. https://doi.org/10.1086/652409.

Nita, G.M., Gary, D.E., & Hellbourg, G. (2016a). Spectral kurtosis statistics of quantized signals. In 2016 Radio Frequency Interference (RFI) (p. 75–80). IEEE. URL: doi: 10.1109/RFINT.2016.7833535. doi:10.1109/rfint.2016.7833535.

Nita, G.M., Gary, D.E., Liu, Z., et al., 2007. Radio frequency interference excision using spectral domain statistics. Publ. Astron. Soc. Pac. 119 (857), 805–827. https://doi.org/10.1086/520938.

Nita, G.M., Hellbourg, G., 2020. A cross-correlation based spectral kurtosis RFI detector. In: In 2020 XXXIIIrd General Assembly and Scientific Symposium of the International Union of Radio Science. IEEE. https://doi.org/10.23919/ursigass49373.2020.9232200.

Nita, G.M., Hickish, J., MacMahon, D. et al. (2016b). EOVSA implementation of a spectral kurtosis correlator for transient detection and classification. Journal of Astronomical Instrumentation, 05(04). URL: doi: 10.1142/S2251171716410099. doi:10.1142/s2251171716410099.

Noorazlan, N., Abidin, Z.Z., Rosli, Z., 2013. Radio frequency interference analysis for potential future very long baseline interferometer in malaysia. In: In AIP Conference Proceedings, pp. 5–10. https://doi.org/10.1063/1.4803558. AIP.

Parsons, J.D., Gardiner, J.G., 1989. Multipath characteristics in urban areas. In: Mobile Communication Systems. Springer, US, pp. 27–67. https://doi.org/10.1007/978-1-4684-1526-1_2.

Pearson, K., Henrici, O.M.F.E., 1895. X. contributions to the mathematical theory of evolution.—II. skew variation in homogeneous material. Philos. Trans. Roy. Soc. London. (A.) 186, 343–414. https://doi.org/10.1098/rsta.1895.0010, URL: https://royalsocietypublishing.org/doi/abs/10.1098/rsta.1895.0010.

Quirós-Olozábal, A., González-de-la Rosa, J.-J., Cifredo-Chacón, M.-A., et al., 2016. A novel FPGA-based system for real-time calculation of the spectral kurtosis: A prospective application to harmonic detection. Measurement 86, 101–113. https://doi.org/10.1016/j.measurement.2016.02.031.

Redoblado, P.A.A.L., Kumar, S., Kumar, A., et al., 2022. Lightning evolution and vlf perturbations associated with category 5 tc yasa in the south pacific region. Earth, Planets and Space 74 (1). https://doi.org/10.1186/s40623-022-01632-3.

Rozhnoi, A., Solovieva, M., Fedun, V., et al., 2019. Strong influence of solar x-ray flares on low-frequency electromagnetic signals in middle latitudes. Ann. Geophys. 37 (5), 843–850. https://doi.org/10.5194/angeo-37-843-2019.

Rumi, G.C., 1960. The D1, D2 layers and the absorption of radio waves. J. Geophys. Res. 65 (11), 3625–3630. https://doi.org/10.1029/jz065i011p03625.

Shafie, M.M., Umar, R., Sabri, N.H., 2021. Statistical analysis of radio frequency interference (RFI) caused by solar radiation during wet and dry. Malaysian J. Fundam. Appl. Sci. 17, 430–436.

Shafie, M.M., Umar, R., Sabri, N.H., et al., 2017. Radio environment analysis at Balai Cerap KUSZA for solar burst study. International Journal on Advanced Science Engineering Information Technology 7, 1441–1447.

Shamsuddin, S.N.A., Shariff, N.N.M., 2022. An analysis of the X1.59 flare and associated events on 3rd July 2021. J. Phys: Conf. Ser. 2287 (1), 012034. https://doi.org/10.1088/1742-6596/2287/1/012034.

Shao, X.-M., Lay, E.H., Jacobson, A.R., 2012. Reduction of electron density in the night-time lower ionosphere in response to a thunderstorm. Nat. Geosci. 6 (1), 29–33. https://doi.org/10.1038/ngeo1668.

Smith, E., Lynch, R.S., Pisano, D.J., 2022. Simulating spectral kurtosis mitigation against realistic radio frequency interference signals. Astron. J. 164 (4), 123. https://doi.org/10.3847/1538-3881/ac7e47.

Steeb, J.-W.W., Davidson, D.B., Wijnholds, S.J., 2016. Spatial filtering of near-field radio frequency interference at a lofar lba station. In: In 2016 Radio Frequency Interference (RFI). IEEE. https://doi.org/10.1109/rfint.2016.7833544.

Stening, R., 1992. Modelling the low latitude F region. J. Atmos. Terr. Phys. 54 (11–12), 1387–1412. https://doi.org/10.1016/0021-9169(92)90147-d.

Sugiyama, K., Jaroenjittichai, P., Leckngam, A., et al., 2022. The 40-m thai national radio telescope with its key sciences and a future south-east asian vlbi network. Proc. Int. Astron. Union 18 (S380), 461–469. https://doi.org/10.1017/s1743921323002909.

Taylor, J., Denman, N., Bandura, K., et al., 2019. Spectral kurtosis-based RFI mitigation for CHIME. J. Astron. Instrument. 08 (01). https://doi.org/10.1142/s225117171940004x.

The Event Horizon Telescope Collaboration, Akiyama, K., Alberdi, A. et al. (2019). First m87 event horizon telescope results. i. the shadow of the supermassive black hole. The Astrophysical Journal Letters, 875 (1), L1. URL: doi: 10.3847/2041-8213/ab0ec7. doi:10.3847/2041-8213/ab0ec7.

Thompson, A.R., Clark, B.G., Wade, C.M., et al., 1980. The very large array. The Astrophysical Journal Supplement Series 44, 151. https://doi.org/10.1086/190688.

Thomson, N.R., Clilverd, M.A., 2001. Solar flare induced ionospheric d-region enhancements from vlf amplitude observations. J. Atmos. Solar Terr. Phys. 63 (16), 1729–1737. https://doi.org/10.1016/s1364-6826(01)00048-7.

Tian-qi, L., Ya-jun, W., Ren-jie, Z., et al., 2021. Study of radio frequency interference mitigation method based on wavelet transform. Chin. Astron. Astrophy 45 (4), 587–599. https://doi.org/10.1016/j.chinastron.2021.11.009.

Tulasi Ram, S., Su, S., Liu, C.H., 2009. FORMOSAT-3/COSMIC observations of seasonal and longitudinal variations of equatorial ionization anomaly and its interhemispheric asymmetry during the solar minimum period. J. Geophys. Res.: Space Phys. 114 (A6). https://doi.org/10.1029/2008ja013880.

Umar, R., Abidin, Z.Z., Ibrahim, Z.A., 2013. The importance of radio quiet zone (RQZ) for radio astronomy. In: In AIP Conference Proceedings. AIP. https://doi.org/10.1063/1.4803564.

Umar, R., Abidin, Z.Z., Ibrahim, Z.A., et al., 2012. Population density effect on radio frequencies interference (rfi) in radio astronomy. In: In AIP Conference Proceedings, pp. 39–42. https://doi.org/10.1063/1.4730683. AIP.

Umar, R., Abidin, Z.Z., Ibrahim, Z.A., et al., 2014. Selection of radio astronomical observation sites and its dependence on human generated rfi. Res. Astron. Astrophys. 14 (2), 241–248. https://doi.org/10.1088/1674-4527/14/2/012.

Umar, R., Sabri, N.H., Ibrahim, Z.A., et al., 2015. Measurement technique in radio frequency interference (RFI) study for radio astronomy purposes. Malaysian J. Anal. Sci. 48.

Wagner, L.S., Goldstein, J.A., Rupar, M.A., et al., 1995. Delay, doppler, and amplitude characteristics of HF signals received over a 1300 km transauroral sky wave channel. Radio Science 30 (3), 659–676. https://doi.org/10.1029/94rs03177.

Widrow, B., Stearns, S., 1985. Adaptive Signal Processing. Prentice-Hall.

Wongphechauxsorn, J., Champion, D.J., Bailes, M., et al., 2023. The High Time Resolution Universe Pulsar survey – XVIII. the reprocessing of the HTRU-S low lat survey around the galactic centre using a fast folding algorithm pipeline for accelerated pulsars. Mon. Not. R. Astron. Soc. 527 (2), 3208–3219. https://doi.org/10.1093/mnras/stad3283.

Yang, Z., Yu, C., Xiao, J., et al., 2020. Deep residual detection of radio frequency interference for fast. Mon. Not. R. Astron. Soc. 492 (1), 1421–1431. https://doi.org/10.1093/mnras/stz3521.

Zafar, S., Zafar, N., Ibrahim, Z., et al., 2018. Spectrum monitoring: Radio frequency interferences (rfi) profile for hydroxyl (oh) lines window. Journal of Fundamental and Applied Sciences 9 (2S), 147. https://doi.org/10.4314/jfas.v9i2s.11.

Zafar, S.N.A.S., Umar, R., Sabri, N.H., et al., 2017. Determination of radio environmental level in hydrogen (HI) band spectrum by using kurtosis analysis. Int. J. Adv. Sci. Eng. Inform. Technol. 7, 1069–1075.

Zavvari, A., Islam, M.T., Anwar, R., et al., 2015. Analysis of radio astronomy bands using callisto spectrometer at malaysia-ukm station. Exp. Astron. 41 (1–2), 185–195. https://doi.org/10.1007/s10686-015-9480-z.

Zhao, B.-X., Zheng, Q., Shan, H.-Y., et al., 2022. North celestial region observed with 21 CentiMeter Array. Res. Astron. Astrophys. 22 (1). https://doi.org/10.1088/1674-4527/ac37b3, 015–012.

Zhou, Y., & Ju, H. (2019). HF sky wave hop-propagation on earth's surfaces in different conditions. Journal of Physics: Conference Series, 1176, 042040. URL: doi: 10.1088/1742-6596/1176/4/042040. doi:10.1088/1742-6596/1176/4/042040.